

Practical Aspects of Collider Physics

Heidi Schellman
Dept. of Physics and Astronomy
Northwestern University
Evanston, IL USA 60208

July 14, 2005

Abstract

A brief overview of experimental collider physics for theoretical physics students, illustrated with recent results from the DØ and CDF experiments at the Tevatron.

Contents

1	Introduction and Acknowledgements	2
2	The characters in the story	2
3	The Technical details	2
3.1	Luminosity	2
3.2	Overview of Collider detectors	4
4	Example 0 - Z-pole at LEP	4
4.1	What we expect to see	7
4.2	The Measurement	7
4.3	Luminosity	11
4.4	Beam Energy	12
4.5	Other corrections	14
5	Hadron Collider physics Basics	16
5.1	The final state	17
5.2	Kinematics	21
6	Example 1: Jet production	23
6.0.1	Hadron Energy Calibration	27
6.1	Result	27
7	Simulations and neutrinos	27
7.1	QCD Backgrounds to rarer processes	28
7.2	Discussion of simulations	31

8	Neutrino detection at colliders	31
9	Example 2: The top quark at the Tevatron	32
9.1	Standard Model top production	32
9.2	Backgrounds	34
9.3	Top mass	36
9.4	Extraction of the top mass	39
10	Example 3: looking for the Higgs at Hadron colliders - or where is it any-ways?	41
10.1	Standard Model Higgs production and decay	41
10.2	Triggers and Detection	44
10.3	The solution	46
11	Conclusions	48

1 Introduction and Acknowledgements

Because these lectures are meant to be educational rather than cutting edge, I have gone into more detail than usual. Such details are usually only available in doctoral dissertations. In particular I have relied on the DØ Dissertations of Levan Babukhadia [21], Robert Snihur [14], Juan Estrada [18] and Florencia Canelli [19].

An earlier version of these notes, for hadron colliders only, was given at TASI04.

2 The characters in the story

These lectures describe physics done at lepton and hadron colliders, which have had several historical phases.

3 The Technical details

3.1 Luminosity

Luminosity measures the flux of particles capable of creating a reaction of interest. The number $N_{observed}$ of events observed in an experiment is

$$N_{observed} = \left[\sigma_{process} \times \epsilon_{detection} \times \int \mathcal{L} dt \right] + N_{background} \tag{1}$$

where the observable $\sigma_{process}$ is the cross section for the process and should not depend on the experimental details, $\epsilon_{detection}$ is the probability that a signal event will be observed in a given detector, $\int \mathcal{L} dt$ is the Integrated Luminosity and $N_{background}$ are events from other processes that got counted incorrectly.

At colliders, the luminosity depends on both the beam intensities and the beam densities.

Accelerator	Location	Process	CM Energy	Dates	Some Expts.	Major results
SPEAR	SLAC	e^-e^+	3-6 GeV	72-90	Mark I, Crystal Ball	Charm, τ , jets
Petra	DESY	e^-e^+	14-46 GeV	78-86	JADE, Tasso, Argus ...	gluon jets, b mixing
PEP	SLAC	e^-e^+	29 GeV	80-90	Mark II, TPC, MAC, ASP	b-lifetime
Sp \bar{p} S	CERN	$p\bar{p}$	540 GeV	81-90	UA1, UA2, UA5	W/Z
Tristan	KEK	e^-e^+	50-64 GeV	87-95	Amy, Topaz, Venus	top has very high mass
SLC	SLAC	e^-e^+	91 GeV	90's	SLC	polarized Z prod. (A_{LR})
LEP	CERN	e^-e^+	91 GeV	89-96	Aleph, Opal, L3, Delphi	high statistics EW
Hera	DESY	ep	30GeV on 900 GeV	92-now	H1, Zeus, Hermes, HeraB	Proton structure, diffraction
Tevatron I	Fermilab	$p\bar{p}$	900 GeV	87-96	CDF, D0	top and W mass
LEP II	CERN	e^-e^+	91-210 GeV	96-00	Aleph, Opal, L3, Delphi	WW production, W mass
Tevatron II	Fermilab	$p\bar{p}$	980 GeV	01 - 09?	CDF, D0	Higgs? Supersymmetry?
LHC	CERN	pp	14 TeV	late 00's	Atlas, CMS, LHCb	Higgs? Supersymmetry?
ILC	??	e^-e^+	500 GeV	late 10's	??	Higgs ? Supersymmetry?

Table 1: Collider experiments at the energy frontier (DORIS, CESR, BES, Belle, Pep II not included)

$$\mathcal{L} = f \frac{N_p N_{\bar{p}}}{4\pi\sigma_x\sigma_y} \quad (2)$$

where f is the frequency with which beam bunches cross (1.7 MHz at the Tevatron), N_p is the number of protons/bunch, $N_{\bar{p}}$ is the number of anti-protons/bunch and σ_x and σ_y are the gaussian sizes of the beam. See <http://www-bd.fnal.gov/notifyservlet/www> for the real-time numbers for the Tevatron. Typical beam sizes at hadron colliders are 20-100 μms and typical instantaneous luminosities are $5 \times 10^{31} \text{cm}^{-2} \text{sec}^{-1}$. For integrated luminosities, we normally use inverse pico-barns (1 pico-barn $^{-1} = 10^{36} \text{cm}^{-2}$) as a unit. During a typical running week, which has around 200,000 seconds of beam in it, 7-10 pb $^{-1}$ of luminosity will be delivered to each of the Fermilab experiments. This means that if a particle has a production cross section of 100 fb, one a week will be produced (but probably not detected) at the Tevatron.

3.2 Overview of Collider detectors

Particle detectors at colliders have evolved to be pretty similar - the technologies used in each component differ but they all have the same basic layout. Starting at the interaction point, there is

- a tracking volume with almost no material and a high magnetic field. This is used to measure the trajectory of charged particles with high precision. It normally has an inner, high resolution section built of silicon to detect the decays of short lived particles and an outer tracker made of less expensive materials and optimized for momentum measurement.
- a 'calorimeter' made of very heavy material which absorbs and detects almost all strongly and electromagnetically interacting particles. It is normally divided in to a high Z electromagnetic part and a cheaper outside hadronic part.
- a muon detection system, which measures the momentum of any muons which make it through the calorimeter.

These different pieces are illustrated in the picture of the DØ detector (Figure 1). More detail on these components is given below.

4 Example 0 - Z-pole at LEP

One of the major accomplishments of the LEP e^-e^+ collider at CERN was the precision measurement of the parameters of the Z_0 boson. The mass, width and production cross section were determined with extreme precision. In addition, decay rates to different final states and parity violating asymmetries were also measured very accurately. These results were so precise that they constrained the top mass in the Standard Model before the top mass was accurately measured. In addition, the width measurement provided a strong limit on the number of active neutrino species (2.97 ± 0.03 last time I checked). The Z_0 mass determination is an order of magnitude better than any other mass determination for a heavy particle and provides a very precise calibration for hadron colliders.

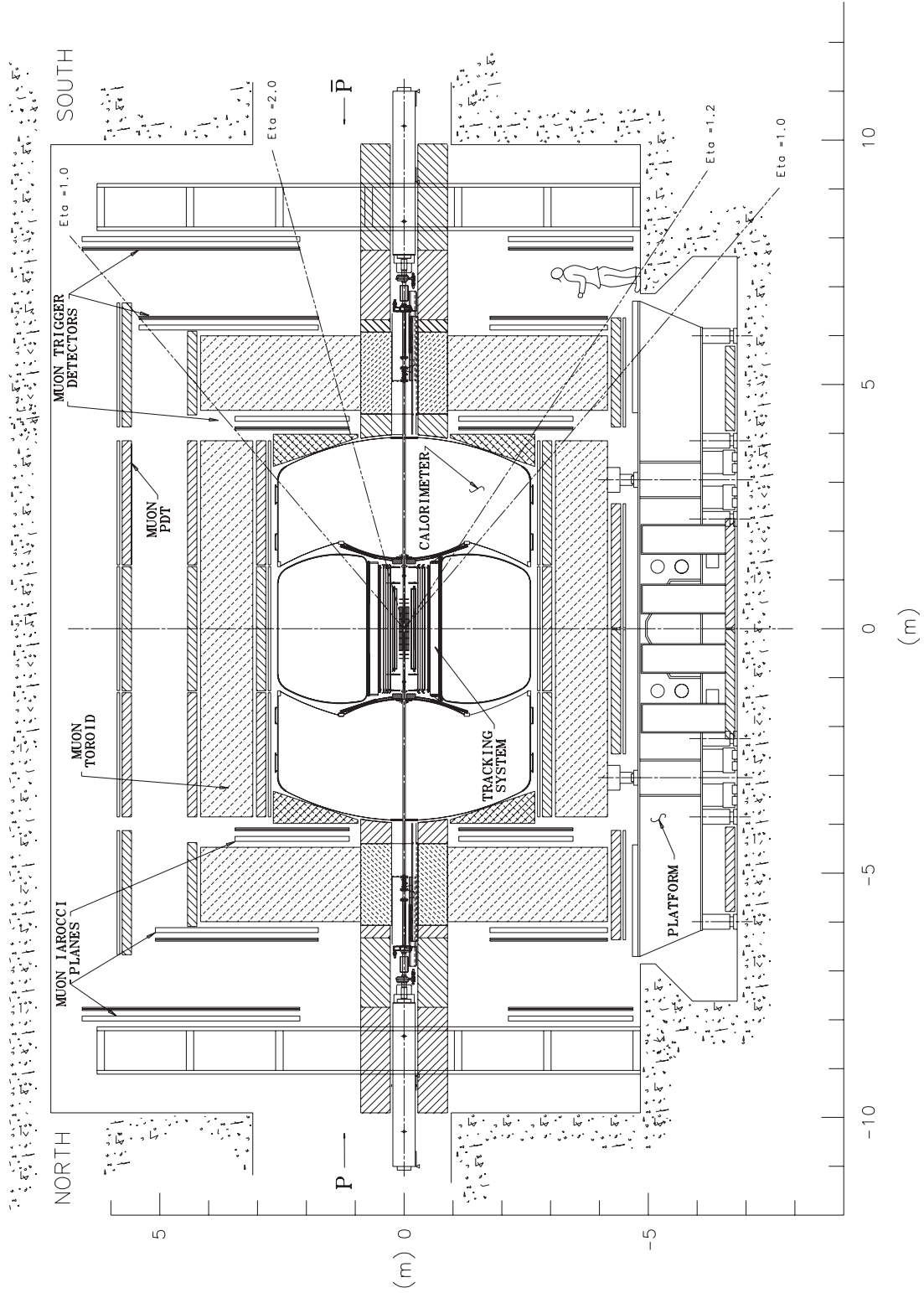


Figure 1: Side view of the DØ detector. The innermost area contains a silicon vertex detector surrounded radially by a scintillating fiber magnetic tracker. The intermediate region is the calorimeter, shown in more detail in the next figure, and the outermost system detects muons which have escaped from the calorimeter.

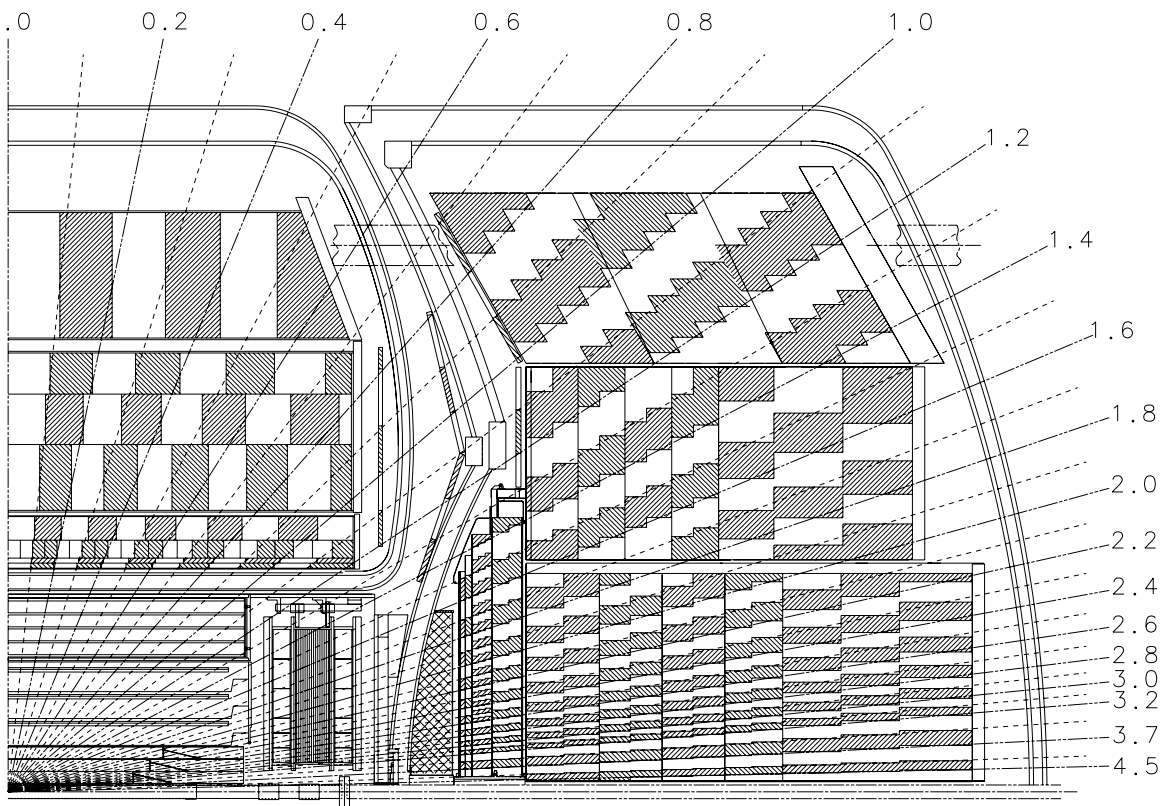


Figure 2: One quadrant of the $D\bar{O}$ calorimeter illustrating the segmentation in pseudorapidity.

4.1 What we expect to see

Z^0 's are produced at LEP through the process $e^-e^+ \rightarrow Z^0 \rightarrow f\bar{f}$ where f are the fundamental fermions. For charged fermion final states there is interference with $e^-e^+ \rightarrow \gamma^* \rightarrow f\bar{f}$. The total width of the Z^0 is

$$\Gamma_{tot} = \Gamma_{e\bar{e}} + \Gamma_{\mu\bar{\mu}} + \Gamma_{\tau\bar{\tau}} + \sum_{i=1, N_\nu} \Gamma_{\nu\bar{\nu}} + 3(\Gamma_{u\bar{u}} + \Gamma_{d\bar{d}} + \Gamma_{s\bar{s}} + \Gamma_{c\bar{c}} + \Gamma_{b\bar{b}}) + \text{anything else} \quad (3)$$

The sum is over the number of neutrino species which couple to the Z^0 , the various Γ 's depend on the couplings to the Z^0 and the factor of 3 for quarks is for the 3 color species. QCD corrections add factors of order α_s to the quark modes due to final stage gluon radiation. Γ_{tot} can be measured from the width of the Z^0 production rate:

The rate for fermion pair production near the Z pole is given by the LEP EWWG [?] as follows.

$$\begin{aligned} \text{„} \frac{2s}{\pi} \frac{1}{N_c^f} \frac{d\sigma_{ew}}{d\cos\theta} (e^-e^+ \rightarrow f\bar{f}) = & \\ & \underbrace{\left| \alpha(m_Z) Q^f \right|^2 (1 + \cos^2 \theta)}_{\gamma} \\ & \underbrace{-8 \operatorname{Re} \left\{ \alpha^*(m_Z) Q^f \chi(s) \left[\mathcal{G}_V^e \mathcal{G}_V^f (1 + \cos^2 \theta) + 2 \mathcal{G}_A^e \mathcal{G}_A^f \cos \theta \right] \right\}}_{\gamma - Z^0 \text{ interference}} \\ & \underbrace{+16 |\chi(s)|^2 \left[(|\mathcal{G}_V^e|^2 + |\mathcal{G}_A^e|^2)(|\mathcal{G}_V^f|^2 + |\mathcal{G}_A^f|^2)(1 + \cos^2 \theta) \right.}_{Z^0} \\ & \quad \left. + 8 \operatorname{Re} \left\{ \mathcal{G}_V^e \mathcal{G}_A^{e*} \right\} \operatorname{Re} \left\{ \mathcal{G}_V^f \mathcal{G}_A^{f*} \right\} \cos \theta \right]} \\ & \end{aligned} \quad (4)$$

$$\chi(s) = \frac{G_F m_Z^2}{8\pi\sqrt{2}} \frac{s}{s - m_Z^2 + i s \Gamma_Z/m_Z} . \quad (5)$$

Here $\alpha(m_Z)$ is the electromagnetic coupling constant at the scale of the Z^0 mass, G_F is the Fermi constant, Q^f is the charge of the final state fermion, and the colour factor N_c^f is one for leptons ($f=e, \mu, \tau$) and three for quarks ($f=u, d, s, c, b$). The effective vector and axial vector couplings of fermions to the Z^0 are denoted by \mathcal{G}_V^f and \mathcal{G}_A^f . $\chi(s)$ is the propagator term characterized by a Breit-Wigner denominator with an s -dependent width. ”

Figure 5 shows the measured variation of the cross section for $e^-e^+ \rightarrow q\bar{q}$ with center of mass energy at LEP. The data were taken at energies selected to both optimize the mass and width measurements and provide the maximum number of Z decays possible in a given running time. The measured width Γ_{tot} is consistent with the known quark and lepton species, with $N_\nu = 3$ and no other particles with masses less than m_Z which couple to the Z^0 .

4.2 The Measurement

To do this measurement you need to determine the cross section at various energies.

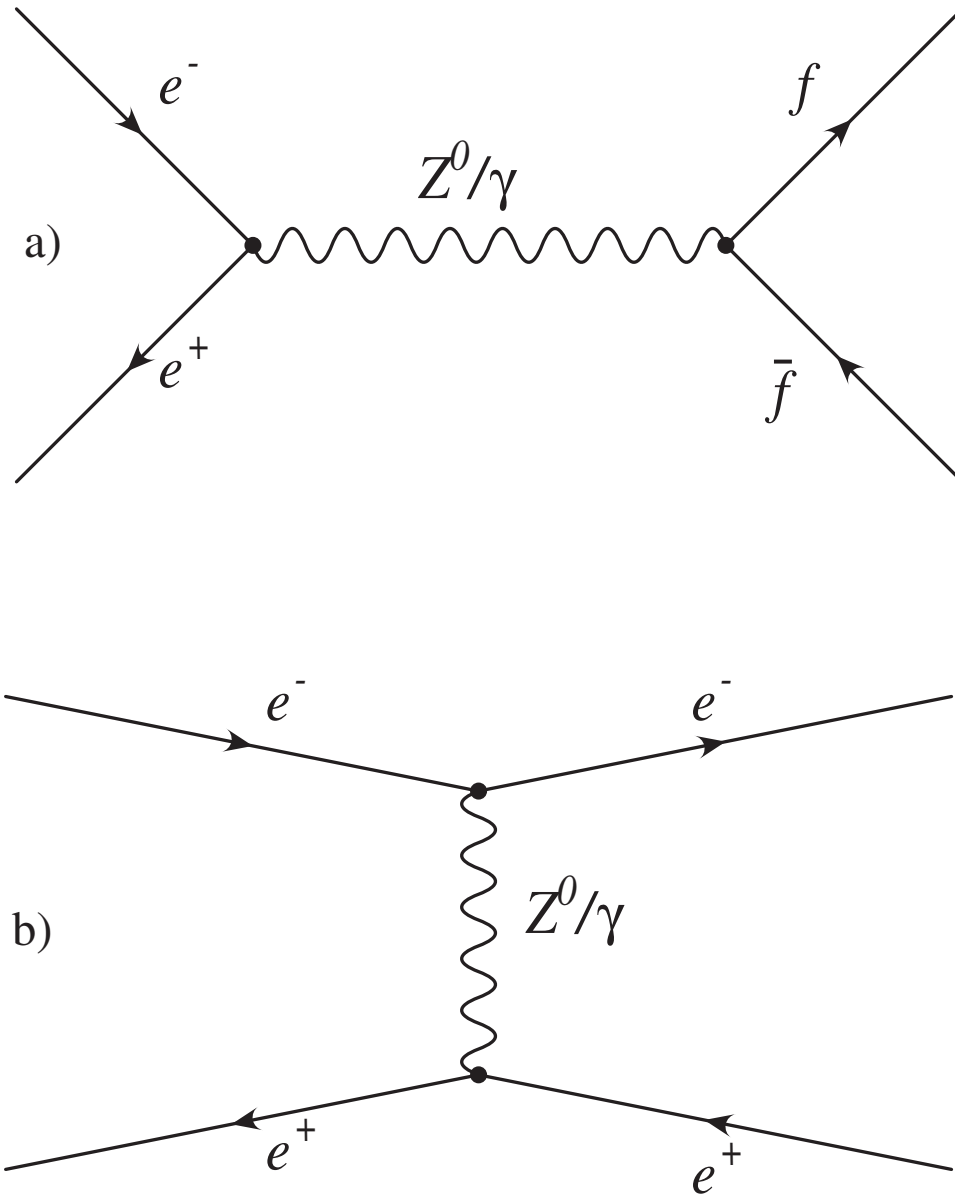


Figure 3: Diagrams for $e^-e^+ \rightarrow f\bar{f}$ through γ or Z^0 . a) shows the s -channel scattering which can have any fermionic final state which couples to the Z or γ . b) shows the t -channel process which only involves the e^-e^+ final state.

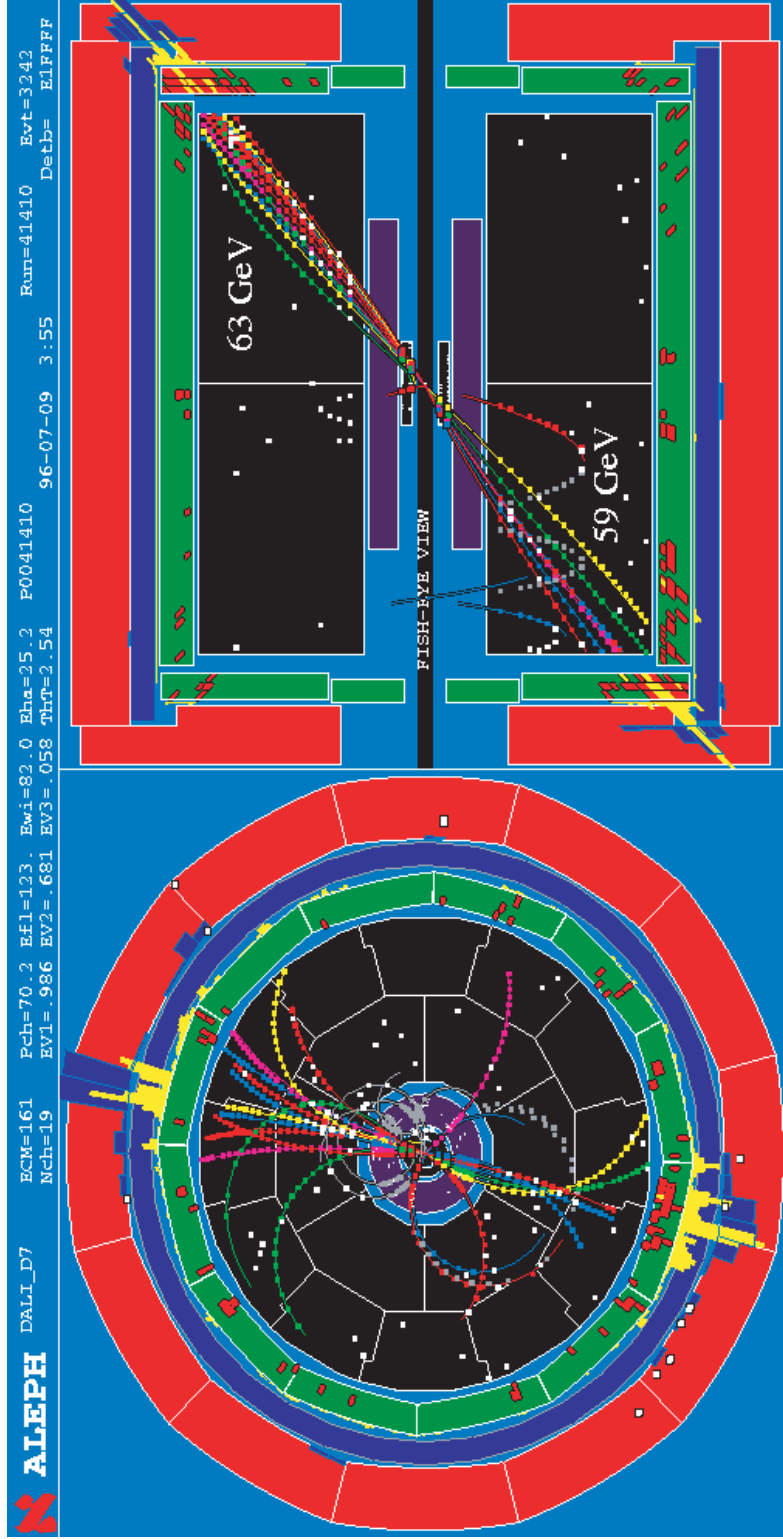


Figure 4: An $e^-e^+ \rightarrow q\bar{q}$ event at the Aleph detector. The Left view is along the beam and magnetic field axes, the right view shows the beam-radial plane

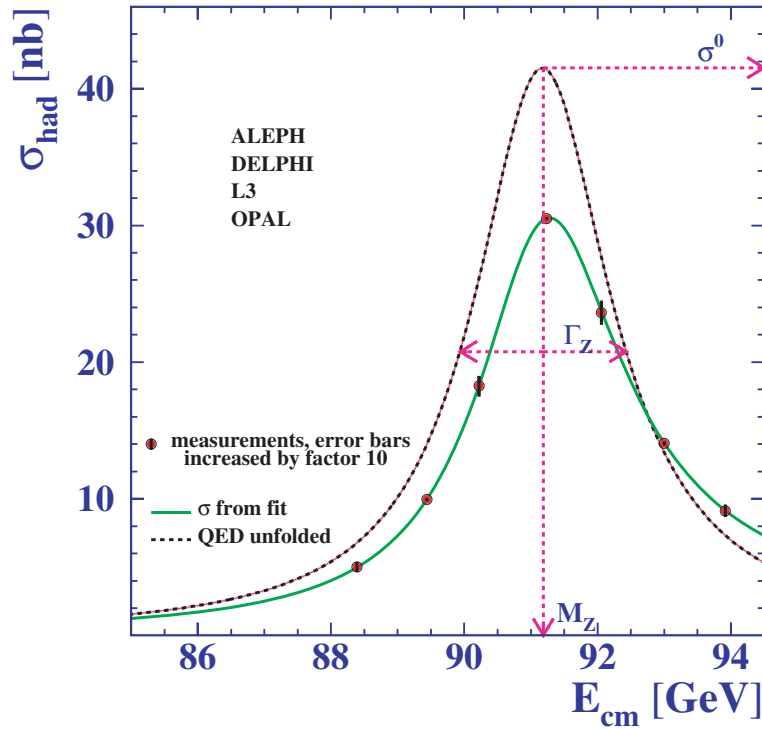


Figure 5: The cross section for hadron production near the Z pole from LEP. The points represent data from the four experiments - with error bars multiplied by a factor of 10, the solid line is a fit to the observed line shape while the dashed line is a fit to the observed data after correction for initial state radiation.

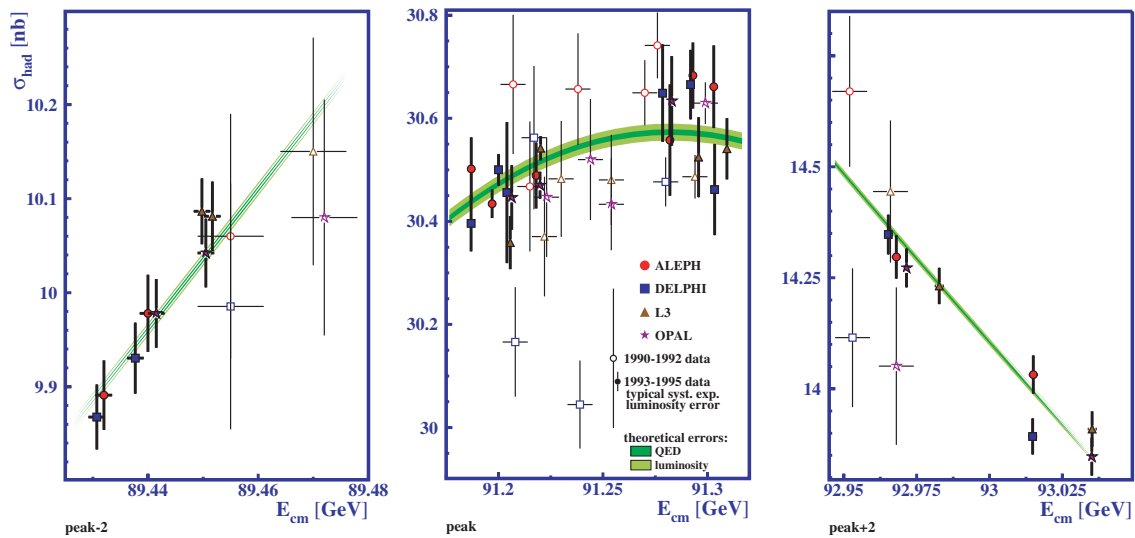


Figure 6: The cross section for hadron production near the Z pole from LEP. The points represent data from the four experiments blown up so that you can see the data and the theoretical curves for the best fit.

The cross section σ for a given process is given by

$$\int \mathcal{L} dt \times \sigma = N_{produced} = \frac{1}{\epsilon} (N_{detected} - N_{background}) \quad (6)$$

where $\int \mathcal{L} dt$ is the integrated luminosity, a measure of the integrated flux of potentially interacting particles, σ is the cross section, $N_{produced}$ is the number of particles produced, which can't be observed. $N_{detected}$ are the number of events seen, $N_{background}$ are the number of events seen which were actually not signal and ϵ is the efficiency or the probability that a produced event will be detected.

The experimental observables are E_{beam} , $\int \mathcal{L} dt$ and $N_{detected}$. $N_{background}$ and ϵ can be estimated from the data or by simulation and with those in hand, one can measure σ .

At LEP, backgrounds are small but efficiencies are not 100%. The efficiency for detecting $e^-e^+ \rightarrow Z/\gamma^* \rightarrow f\bar{f}$ was determined for quarks, muons, taus, and electrons using precision simulations which had been tuned to the observed data. The dominant part of the efficiency was the 'acceptance', which describes the angular coverage of the detector. Detectors cannot cover all of 4π solid angle so the data are limited to some smaller angular region and theory/simulation are used to extrapolate to 4π . In addition, other forms of inefficiency can occur - some decay modes may be more difficult to reconstruct than others and some parts of the detector may not be working well. These effects are estimated by studying distributions such as the number of hits on tracks and the angular distribution in azimuth. Backgrounds were very low but were also estimated by simulation. The numbers of detected Z^0 candidate events were of order 1-4 million depending on the process. So $N_{observed}$ could be determined pretty easily by counting events with $e^-e^+ \rightarrow f\bar{f}$.

4.3 Luminosity

The Luminosity is an estimate of the fluxes of e^-e^+ which could potentially cause an interaction. In principle this could be calculated from beam spot sizes and currents using equation 1, but in practice these are not measured well enough.

Instead, small angle electron scattering, where the t channel process dominates and hence is dominated by photon exchange, is used as a reference process.

The rate for observing such scattering in a small solid angle $\Delta\Omega$ is

$$\int \mathcal{L} dt \frac{d\sigma(ee)}{d\Omega} \Delta\Omega = \epsilon (N_{detected}^{ee} - N_{background}^{ee}) \quad (7)$$

$\frac{d\sigma}{d\Omega}(ee)$ is estimated from QED, $\Delta\Omega$ and ϵ are very carefully estimated by accurate measurement ($\Delta\Omega$) and simulation (ϵ) and $\mathcal{L} dt$ can be thus be determined and used in extracting $\sigma(e^-e^+ \rightarrow f\bar{f})$. The OPAL collaboration was able to determine this luminosity to 0.03% experimentally with a 0.06% error due to the theoretical cross section for $e^-e^+ \rightarrow e^-e^+$ [8].

Figure 7 shows an engineering drawing of the OPAL luminosity monitor, which wraps around the beam and is made of tungsten plates interleaved with silicon wafers with energy and position readout.

Figure 8

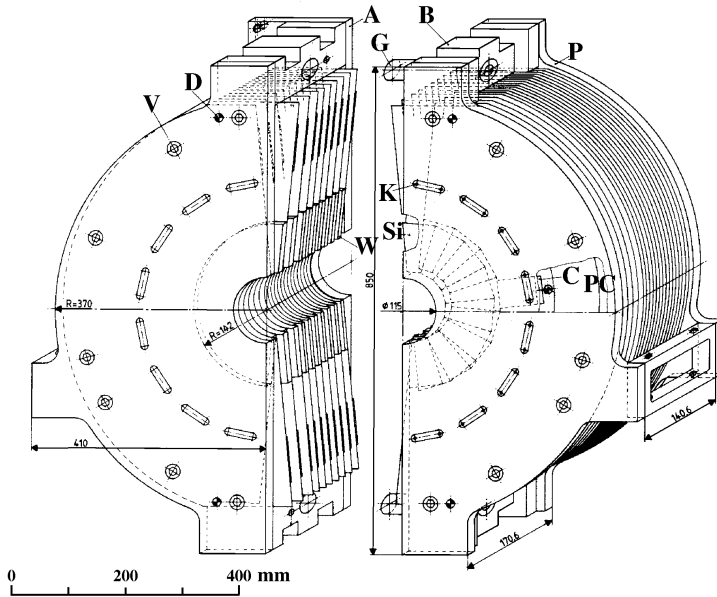


Figure 7: The OPAL luminosity monitor detector.

4.4 Beam Energy

The beam energy at LEP was known, in the end, to a couple of MeV or one part in 20,000[5]. This is not true at most accelerators and is due to a special feature of the LEP machine, the beams become transversely polarized over time and those spins precess. The polarization can be measured by Compton scattering a laser beam from the electron and positron beams. The precession frequency is closely related to the beam energy via the relation

$$E_b = \frac{\nu_s m_e c^2}{(g - 2)/2} \quad (8)$$

where E_b is the beam energy and ν_s is the number of precessions per revolution in the machine. At the Z peak, ν_s was around 103.5. The precession frequency was measured by applying a known RF signal to the beam and sweeping through nearby frequencies, when the correct frequency was reached, the beams would become depolarized.

This establishes the average beam energy around the ring at the time the frequency scan was done. To establish the beam energy at the interaction regions (IP's) at all times, corrections need to be made for:

- Location around the ring, since synchrotron radiation results in 125 GeV energy loss/turn which is restored by RF cavities at fixed locations, see Figure 9. You can also see these shifts in Figure 6 where certain experiments have different energies than others.
- Temperature, which causes expansion of components. It is kept constant to 0.1°C .
- Stray currents caused by the TVG trains which cause a 1A current in the LEP ring. See Figure 10
- Tidal stretching of the earth, which changes the effective radius of the machine

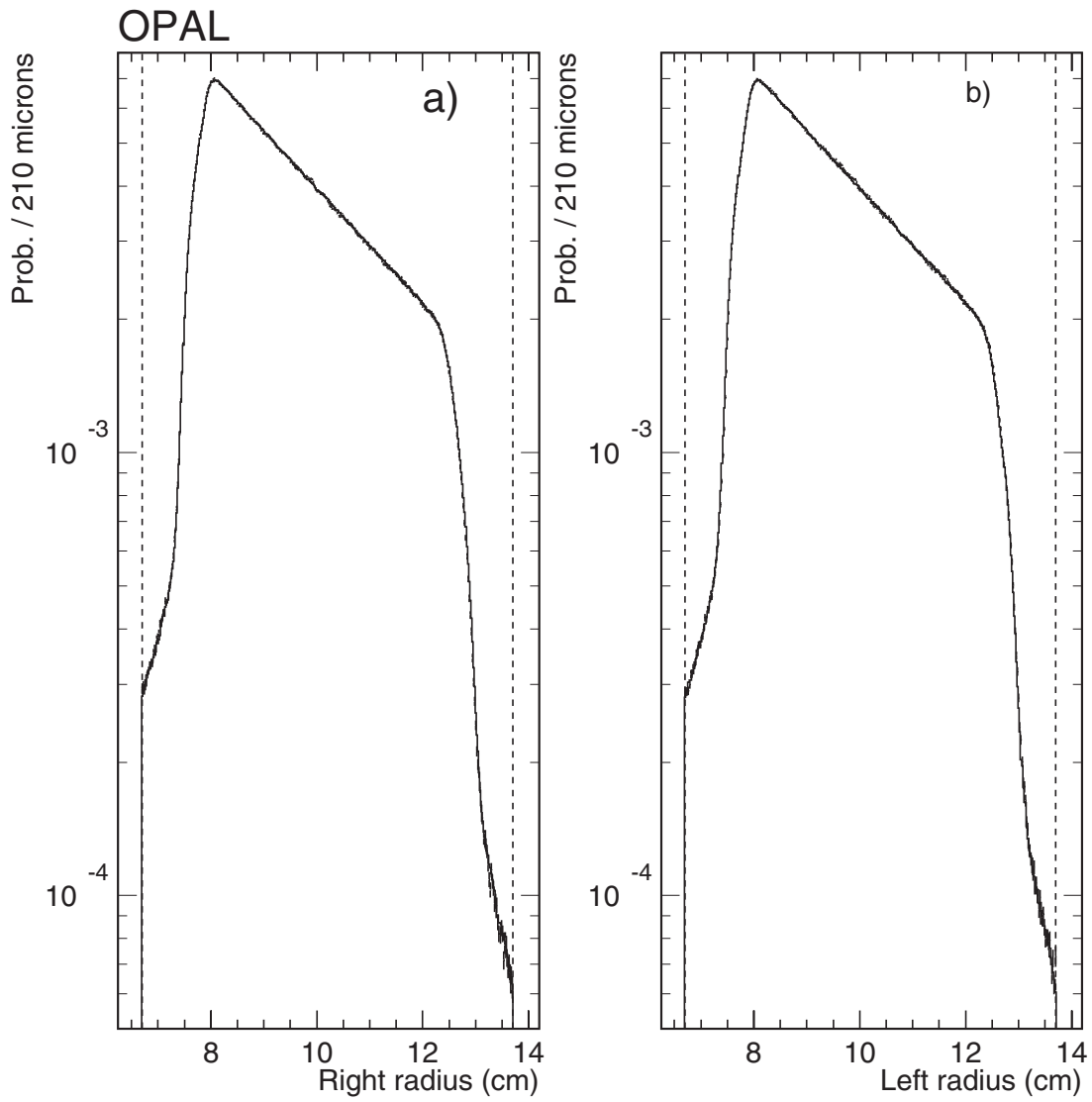


Figure 8: Data from the detector, counts in the detector as a function of radius - the dropoffs indicate the edges of the acceptance of the detector.

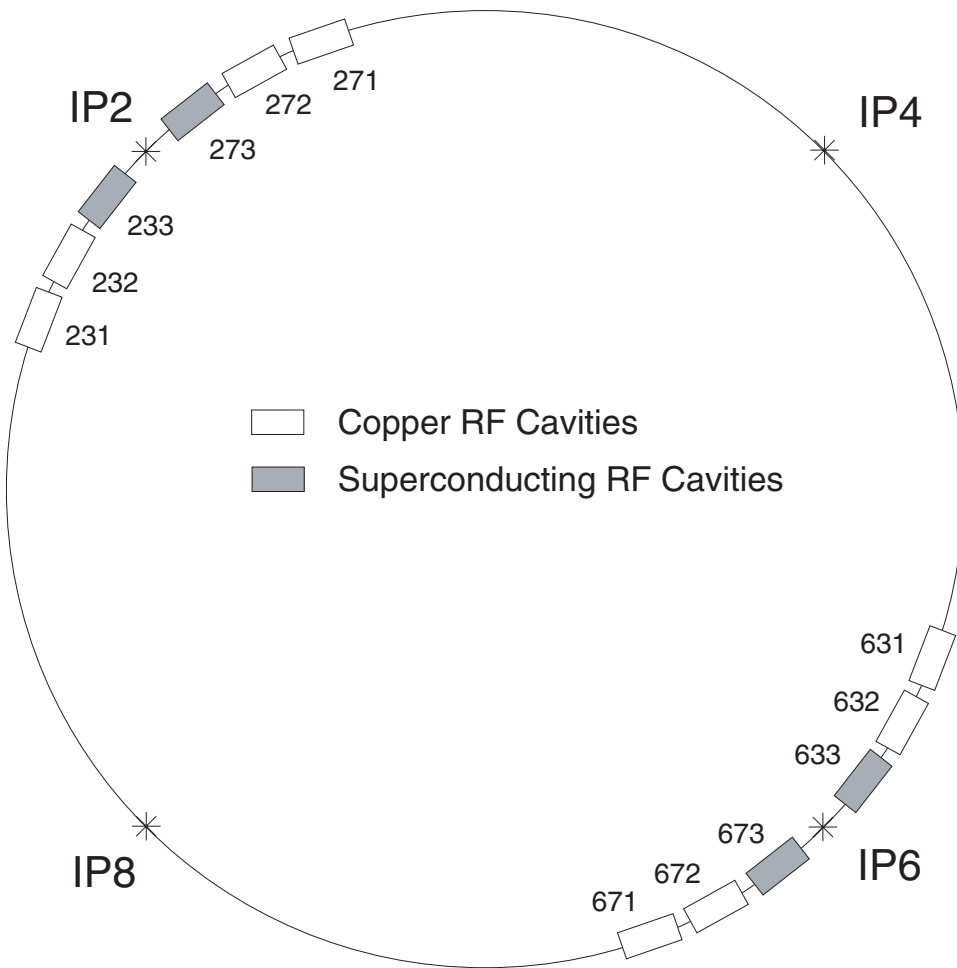


Figure 9: The LEP ring layout. Power is added to the beams in the RF cavities but 125 MeV is lost to synchrotron radiation every turn. Since the RF cavities are not evenly spaced, the beam energy at different Interaction Points (IP's) will differ by up to 40 MeV.

These corrections are described in detail in reference [5].

4.5 Other corrections

Event counting, energy calibration and luminosity measurements get us to the data points shown in Figure ???. Additional corrections are made for initial and final state QED radiation and a combined fit, including the correlations between observables is done. The results of that fit are the dashed curve in Figure ??. This fit to the data from all 4 experiments yields a Z^0 mass of 91.1874 ± 0.0021 MeV, $\Gamma_Z = 2.4952 \pm 0.0023$ GeV and $N_\nu = 2.9841 \pm 0.0083$. with no room for other particles which couple to the Z .

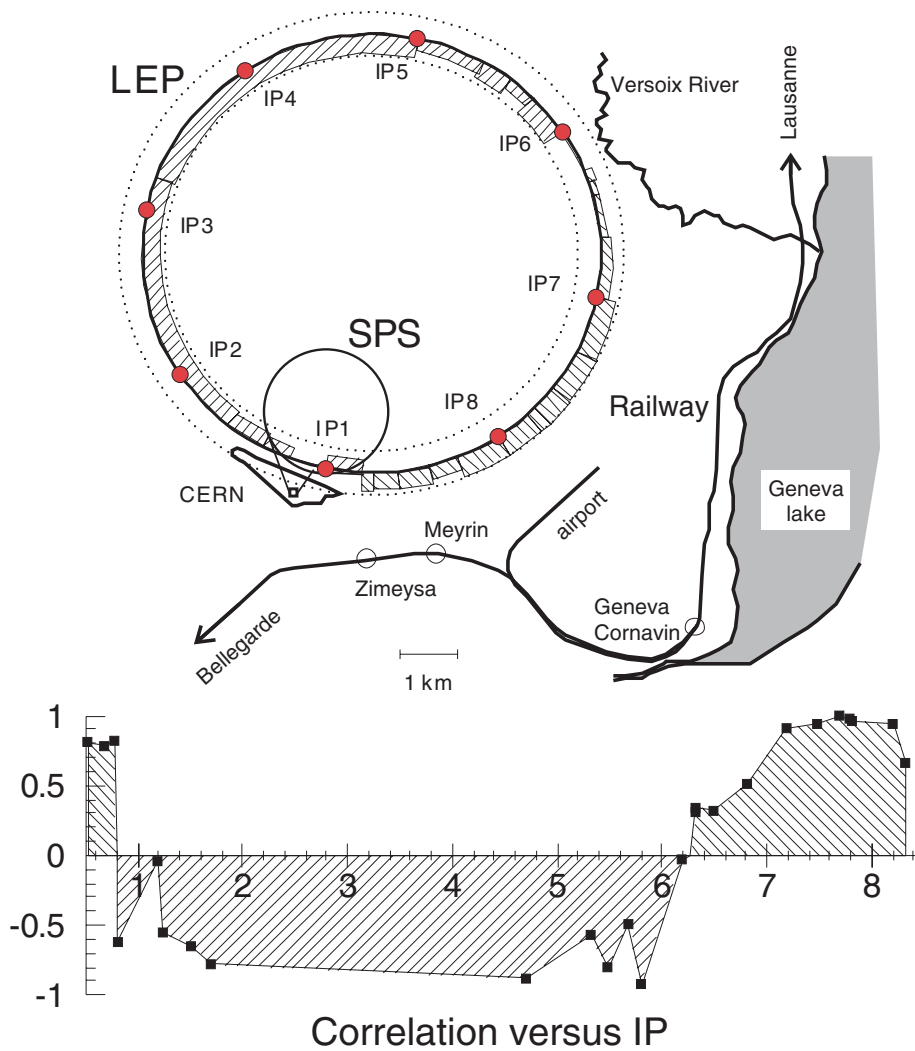


Figure 10: The TVG train line in relation to the LEP ring. The ground return for the train includes the LEP ring and has an effect of order 1-3 MeV on the effective beam energy.

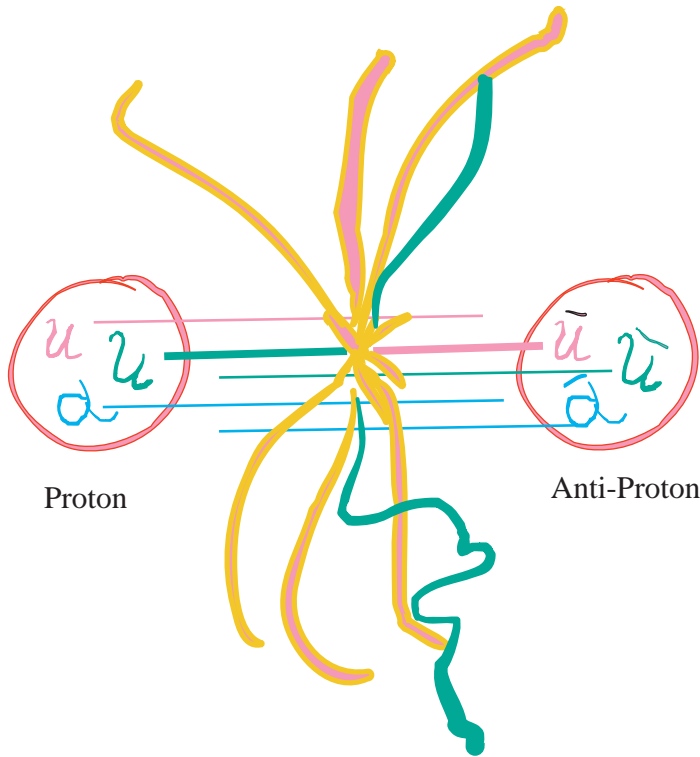


Figure 11: What is really going on in a hadron collider, partons collide and a mess of target remnants and scattered particles ensues. In this event a u from the proton and \bar{u} from the anti-proton have produced a final state with many particles, mainly concentrated in two jets.

5 Hadron Collider physics Basics

As theorists, you think of processes as one or two incoming fundamental particles interacting to form an interesting final state. In e^-e^+ physics this is a good approximation, but in hadron colliders it is an approximation and it turns out, a bad one. Most of my examples will be from proton anti-proton collisions at the Tevatron (since that's what I know) but I will include comments on the LHC which will collide protons with protons.

The problem is that your fundamental incoming partons, quarks and gluons, are delivered in protons and antiprotons. The hard collision of interest only occurs when partons with the right quantum numbers happen to have the right center of mass energy to make the desired final state. Most of the time, the hard collision involves partons with the wrong quantum numbers or the wrong energy and all you get, from your point of view, is junk. The longitudinal momentum distribution of the desired partons in the proton is described by Parton Distribution Functions or PDF's, which can be determined from other processes. But these are probabilities, not certainties. As a result, in a given proton-antiproton reaction you do not know the longitudinal momentum of the initial state although you can predict the distribution of such momenta for an ensemble of events. Figure 12 shows typical parton distribution functions for important partons such as u quarks and gluons.

The total cross section for a parton of type 1 and a parton of type 2 to scatter is the integral over the probability of finding those partons in the proton to begin (the PDF) with times the

hard scattering matrix element. In the following, the hatted quantities refer to the hard parton scatter while the unhatted quantities are for the proton/ antiproton system.

Since we don't know the longitudinal momentum for the initial state, we should use cylindrical coordinates. Unless the protons are polarized, the cross section should be symmetric in azimuth so the relevant variables are p_{\parallel} and p_{\perp} . The parton distributions can be written as

$$f_i(x; \mu) \tag{9}$$

where i is the parton flavor, $x = p_{parton}/p_{proton}$ is the fraction of the proton momentum carried by the parton and μ is an appropriate hard scattering scale for the interaction. In the absence of strong interactions between the quarks in the proton, the PDF's would be just a function of x but interactions introduce a $\log \mu$ dependence.

$$\sigma(p + \bar{p} \rightarrow X) = \int \hat{\sigma}(1 + 2 \rightarrow X; \mu) f_1(x_1; \mu) f_2(x_2; \mu) dx_1 dx_2 \tag{10}$$

$\hat{\sigma}$ is the quark scattering cross section, it depends on the scale μ but (in principle) the observable cross section σ does not. In practice, one guesses that μ is the hard scattering momentum scale Q , which is often assumed to be the mass (*c) of the final state object or the transverse momentum of the final state particles. For a detailed discussion you might wish to look at the CTEQ Handbook of Perturbative QCD [11] or other QCD texts.

The parton center of mass energy is:

$$\hat{s} = x_1 x_2 s = x_1 x_2 (2P_{beam})^2 \tag{11}$$

and the momentum of the parton center of mass is:

$$p_z(cm) = (x_1 - x_2) P_{beam} \tag{12}$$

$$p_{\perp}(cm) \simeq 0 \tag{13}$$

Figure 13 shows the first order hard scattering diagrams for proton anti-proton scattering. Figure 14 shows the typical x and Q ranges for different experiments.

Figure 12 shows typical parton distribution functions at collider energies. If you look at the parton probabilities in Figure 12, you note that gluons are the most probable partons, except at the highest momentum fractions, and in fact, the cross section at very low p_{\perp} is dominated by gluon-gluon and quark-gluon scattering via the t channel.

5.1 The final state

Quarks and gluons do not appear as particles in the final state, instead they fragment into 'jets' of reasonably long-lived hadronic particles such as π^+ , π^- , π^0 , K^+ , K^- , K_L , K_S , η , η' , p , n etc. The π^0 , η decay quickly into photons. This jet of particles generally follows the path of the original quark or gluon but there are important problems in making that identification. These include:

- The final state particles are color neutral, while the quarks and gluons are not. This means that there is a color connection between the final state partons (and the remnants of the proton and anti-proton in most cases).

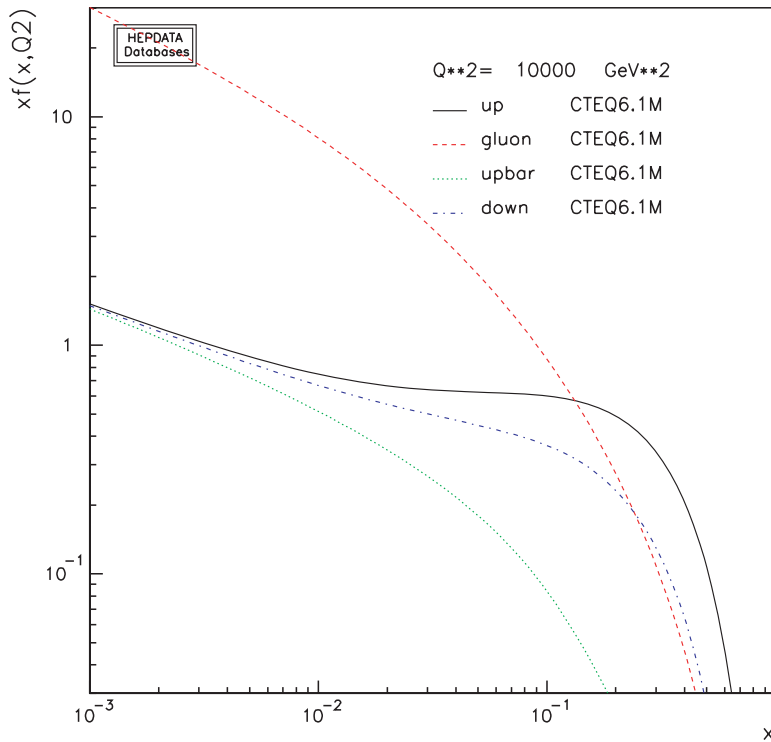


Figure 12: The parton distribution functions (times x) for u quarks (up), d quarks (down), Gluons (gluon) and u anti-quarks (upbar) at a typical collider momentum transfer of $Q = 100\text{GeV}/c$. This was generated with the online pdf plotter from the Durham database <http://durpdg.dur.ac.uk/HEPDATA/PDF>.

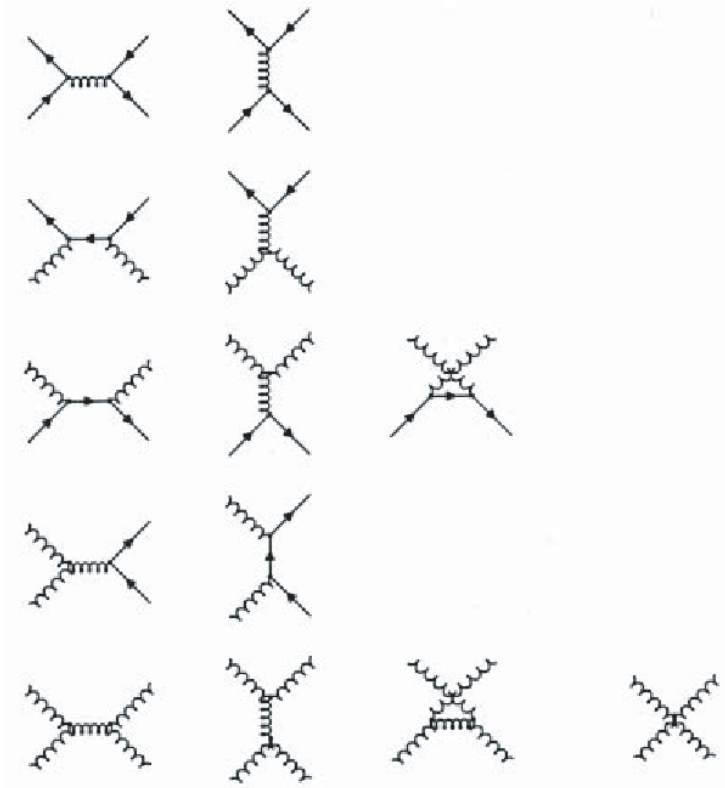


Figure 13: First order diagrams for proton-anti-proton scattering. If one assumes that time runs bottom to top (the theorist's convention), the first column indicate exchange in the t channel, the second s channel exchange, the third the u channel and the 4th is a special QCD diagram.

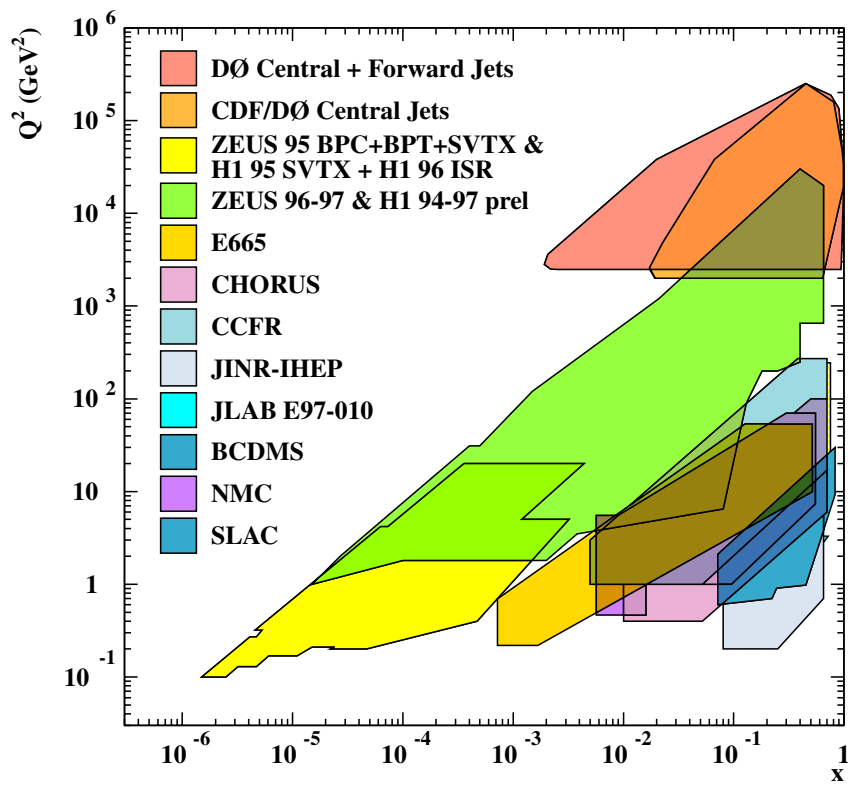


Figure 14: Kinematic coverage of various experiments.

- Higher order diagrams cause jet splitting. Some models of jet production take only the leading order hard diagram and then do fragmentation of those jets using parton shower models while others attempt to include higher order hard scattering diagrams and then fragment them. The degree to which fragmentation is handled in the original matrix element or in the fragmentation model is a rapidly evolving art form.
- Algorithms for finding the jets vary - generally fast algorithms such as cones are hard to map onto theoretical observables while algorithms which are theoretically robust, such as the k_{perp} algorithm, are time consuming and prone to experimental biases. For a nice recent review see reference [16].
- The final state particles deposit energy in the detector in different ways - finding and summing the energy can be quite difficult.

Figure 15 shows the production of a jet when a quark is knocked out of a proton (by a neutrino). In step a), the quark is knocked out but remains connected to the proton by its color charge. At some point the energy in the color field becomes so high that it is energetically favorable to produce a quark anti-quark pair b) which can neutralize some of the color field. In c) the color neutral objects have 'hadronized' to form real observable particles, in this case a neutron and two kaons.

5.2 Kinematics

You may, personally, be interested in Higgsino production but the total proton anti-proton scattering cross section is dominated by t channel exchange of a gluon. Because the backgrounds are dominated by t channel processes, which have factors of $1/t \propto \sin^{-2} \frac{\theta}{2}$ in the matrix element it was realized early on that the polar angle θ was a lousy variable for describing what one actually sees in most produced events, even though most interesting interactions involve s channel quark anti-quark annihilation.

Instead of the polar angle, the rapidity, y , is used.

$$y \equiv \frac{1}{2} \left(\frac{E+p_{\parallel}}{E-p_{\parallel}} \right) \quad (14)$$

$$E = \frac{1}{2} e^y \sqrt{m^2 + p_{\perp}^2} \quad (15)$$

The big deal about rapidity is that:

- Differences in rapidity Δy are Lorentz invariant for boosts along the z (or rapidity) axis. You can verify this for yourself. Because of this, Lorentz Invariant Phase Space can be written as

$$\frac{d^3 p}{2E} = d\phi dy dp_{\perp}^2 = 2\pi dy dp_{\perp}^2 \quad (16)$$

- and if you go to a frame where the rapidity of a final state object is 0, it has a polar angle of $\frac{\pi}{2}$ and small variations in y are

$$\delta y \approx \delta\theta + \mathcal{O}(\delta\theta)^3 \quad (17)$$

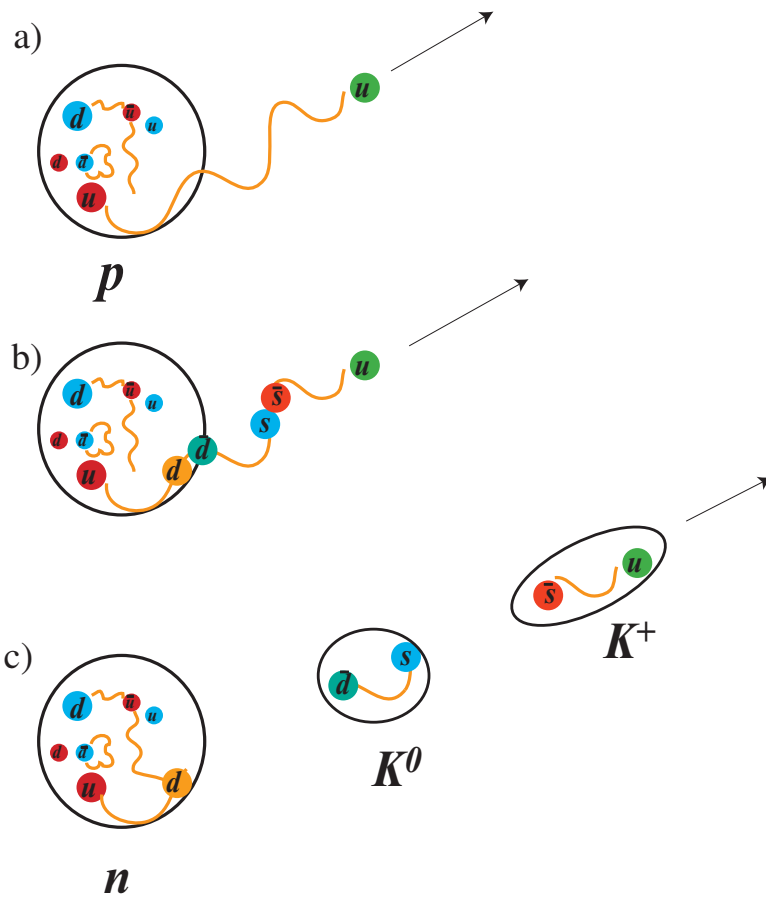


Figure 15: Illustration of fragmentation when a quark is knocked out of a proton, for example in a neutrino interaction.

equivalent to small variations in the polar angle θ .

This means that one can define 'jet's of hadrons in $y - \phi$ space and achieve results similar to those one would get at 90° in $\theta - \phi$ space.

The rapidity of a particle of mass M has kinematic limits set by the total energy available for that particle.

$$E_{max} \geq \frac{1}{2} e^{y_{max}} M \quad (18)$$

$$y_{max} = \log \frac{\sqrt{s}}{M} \quad (19)$$

For example, at the Tevatron, Z^0 bosons will have rapidities of less than 3, while top quarks will be less than 2.3.

The actual rapidity distributions are determined by the product of parton distributions, which determines the longitudinal momentum distributions of interactions, but empirically, the rapidity distribution for soft processes is closely approximated by a constant distribution per unit rapidity within the kinematics limits.

For massless particles (which are a good approximation for the decay products of almost anything in a collider) , the rapidity y reduces to the pseudo-rapidity:

$$\eta = -\log\left(\tan \frac{\theta}{2}\right) \quad (20)$$

Figure 1 shows a side view of the DØ detector at Fermilab. Figure 2 shows a quadrant of the calorimeter and illustrates the segmentation in pseudo-rapidity. Collider detectors are designed so that each detector element covers the same area in $\eta - \phi$ space. For example, at DØ the detector elements are 0.1×0.1 in size.

The utility of plotting things in $\eta - \phi - p_{perp}$ space is illustrated when one looks at real data. Figure 17 shows a normal space view of the objects detected in a very high energy parton scatter. The initial state partons carried more than half of the proton's momentum and scattered at around 90 degrees. Figure 18 shows a lego plot in $\eta - \phi - p_\perp$ coordinates of the energy flow in the final state. Figure 16 illustrates the different coordinate systems and their relationship.

6 Example 1: Jet production

Our first example will be the simple partonic scattering illustrated in Figure 13, where two initial state partons scatter into two or more final state partons. These results have been published in references [17], [22]. Levan Babukhadia's thesis [21] contains a full description of the methods used. The observed final state will consist of 2 or more jets. Because the major diagrams have matrix elements that go like $1/t$ or $1/s$ which act like $1/p_\perp^2$ and the parton distributions approximately go as $1/x(1-x)^n$, the jet spectrum falls off very rapidly with transverse momentum.

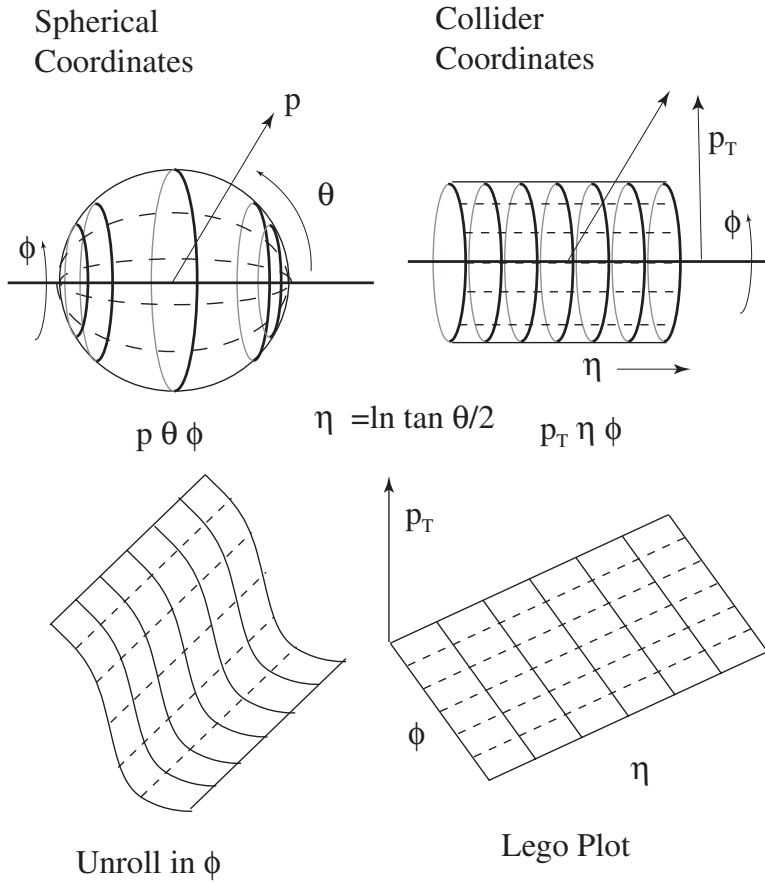


Figure 16: Illustration of collider coordinates. The sphere at top left has lines drawn at rapidity intervals. The cylinder on the right is the same space after the transformation to rapidity space $\theta \rightarrow \eta$. The bottom left diagram shows the cylinder being unrolled to make an $\eta - \phi$ grid. Particles can then be plotted in $\eta\phi p_{perp}$ space.

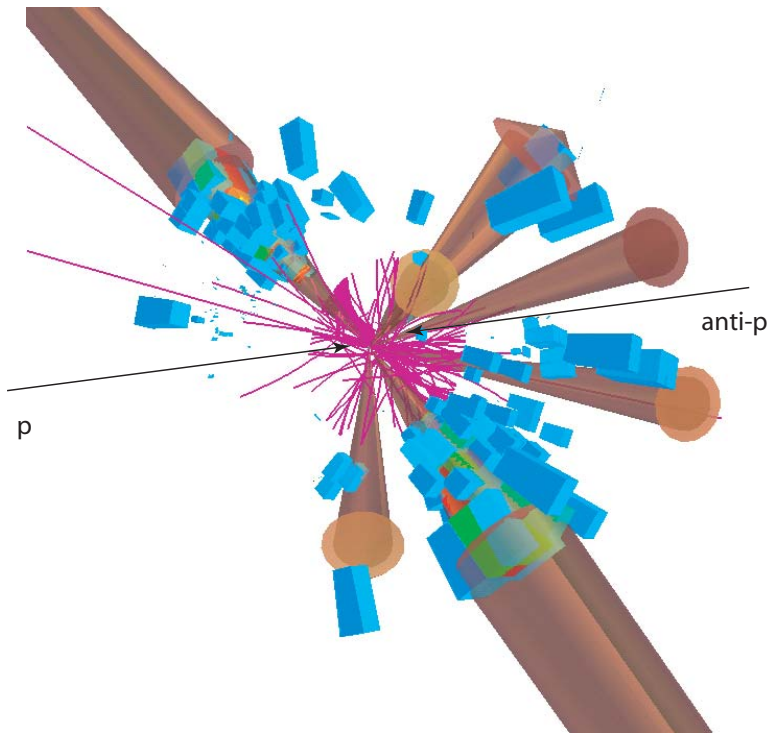


Figure 17: A very high energy event in the DØ detector. The boxes represent calorimeter towers, with blue boxes having higher energy than green ones, the purple line are charged tracks, the brown cylinders are momentum vectors for the jets. The momentum vector scale is set very low, the two largest jets extend far outside the picture.

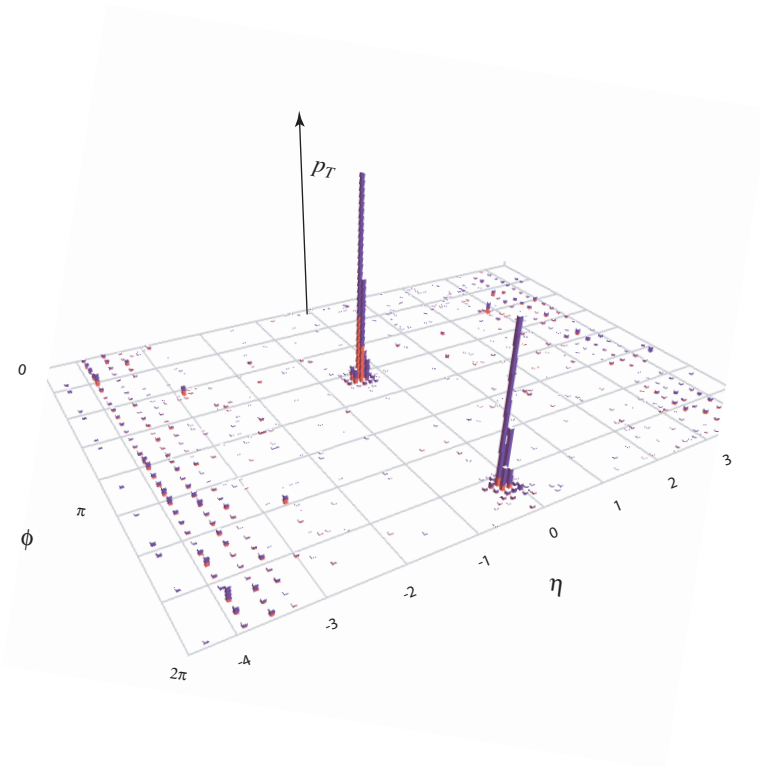


Figure 18: A lego plot of the same event. The calorimeter transverse momentum is plotted in $\eta - \phi$ coordinates. The two high energy jets are very visible. The strange patterns for $|\eta| > 3$ are due to energy deposited by the beam particle remnants and a change in segmentation from 0.1 units to 0.2 in the far forward region.

6.0.1 Hadron Energy Calibration

Nature does not provide very many jet calibration lines. For example, the W and Z bosons decay to jets most of the time but the dijet cross section shows no appreciable enhancement around the mass peaks both due to poor resolution and a factor of $(\frac{\alpha}{\alpha_s})^2$ in electroweak cross sections relative to the QCD cross section. In future, when statistics are higher, the hadronic decays of W 's in top decays should become a promising calibration point with much less background.

Jet scales are found either by a combination of Monte Carlo simulation and test beam measurements for individual particles or by in situ measurement of transverse momentum balance between photons and jets from the QCD/QED process $qG \rightarrow q\gamma$. After enormous effort, errors of the order of 3% on the energy scale can be achieved. [20] is a 94 page article describing the procedure used by D0. 3% sounds good until you remember that the jet spectrum is falling very quickly as a function of the jet transverse momentum. This 3% error on the x (transverse momentum) axis quickly becomes a 30-50% error on the y (cross section) axis when the spectrum is falling fastest.

6.1 Result

Figures 19 and 20 summarize the results from a measurement done at DØ in the late 90's. It is described in great detail in Levan Babukhadia's thesis [21]. The D0 result and a similar measurement from CDF have been published [17, 22]. Figure 19 shows the p_\perp spectrum of jets for several rapidity bins. Figure 20 the p_\perp spectrum normalized to different theoretical predictions. The main source of variation in theoretical predictions is the input parton density functions, in particular, the gluon content at high x which is not well constrained by other experiments. The uncertainty on the measurement is completely dominated by the jet energy scale. What the plot does not show is that error is very highly correlated from point to point.

One can note that the MRST \uparrow g PDF set does match the data more closely and a full statistical analysis indicates that the better match is in fact significant. This has been interpreted as the presence of a larger gluon distribution at high x than had previously been believed. In particular, it indicates that a large fraction of the momentum of the proton can end up in a single gluon.

7 Simulations and neutrinos

Now that we've seen the QCD cross sections, we might want to look at how the others compare. Figure 21 shows the event rates for various processes in hadron-hadron collisions.

All other processes have much lower rates than the QCD rates discussed above and have to contend with huge backgrounds from simple QCD scatters in which the final state particles mimic something more interesting. For example, a W boson can decay to an electron and a neutrino, each with an energy of around 40 GeV in the W center of mass frame. This leads to electrons and neutrinos with transverse momenta in the range 0-40 GeV, depending on the decay angle relative to the beam axis. The total cross section for this process at the Tevatron is around 2.6 nb once you take into account the branching fraction to electrons. The QCD cross section for producing 2 partons with transverse momenta of 25-40 GeV or above is roughly

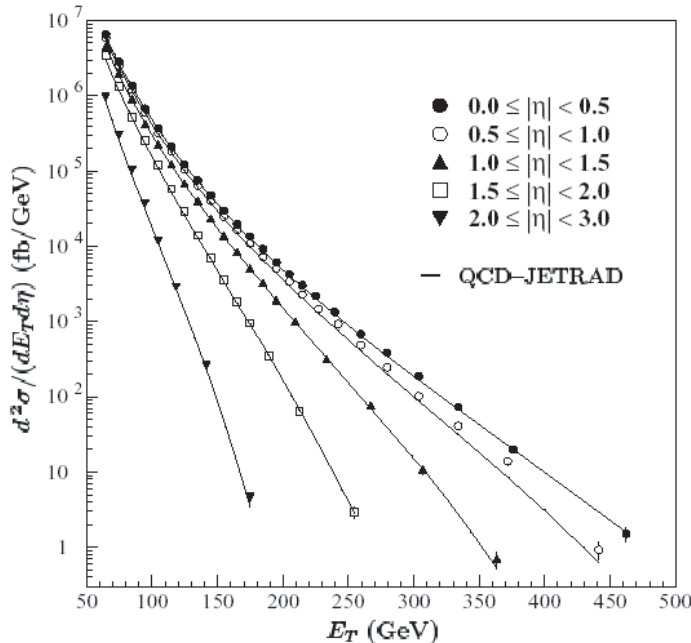


Figure 19: The transverse momentum spectrum for jets produced at center of mass energy 1800 GeV in the D0 detector.

2-10 μbarn or roughly a factor of a thousand higher. If your detector has a 0.1% chance of calling a QCD jet an electron, and messing up its transverse energy, you may be looking at a background as large as your signal. We have better ways of detecting W which will be described later, but one has to be very careful in detector design to measure rare processes in the presence of such large backgrounds.

7.1 QCD Backgrounds to rarer processes

There are several ways in which a normal quark can fragment in a way which looks like an electron, muon or neutrino in a detector.

- Jet fluctuations - a jet of cm energy $E > 40$ resulting from a quark or gluon will have an average number $N_{chg} \simeq 7.7 \log_{10}(E/10 \text{ GeV}) + 1.3$ [27] charged particles, mainly charged pions, and around $N_{neu} \simeq N_{chg}/2$ neutral pions in it. The neutral pions decay to two photons and hence look electromagnetic. Statistical fluctuations¹ can lead to N_{chg} being much smaller than the average, or the relative neutral and pion ratios changing radically in a small fraction of events. A small fraction of jets can either be intrinsically highly electromagnetic and electron like or have a single very energetic charged pion and little else.
- Decay in flight - pions and kaons in the jet can decay in flight, mainly to muons.
- Dalitz decays and Photon interactions in the detector. A π^0 can decay to two photons and one can interact in the detector to form an electron-positron pair.

¹Which are not Poisson in N due to charge and flavor correlations, but even broader.

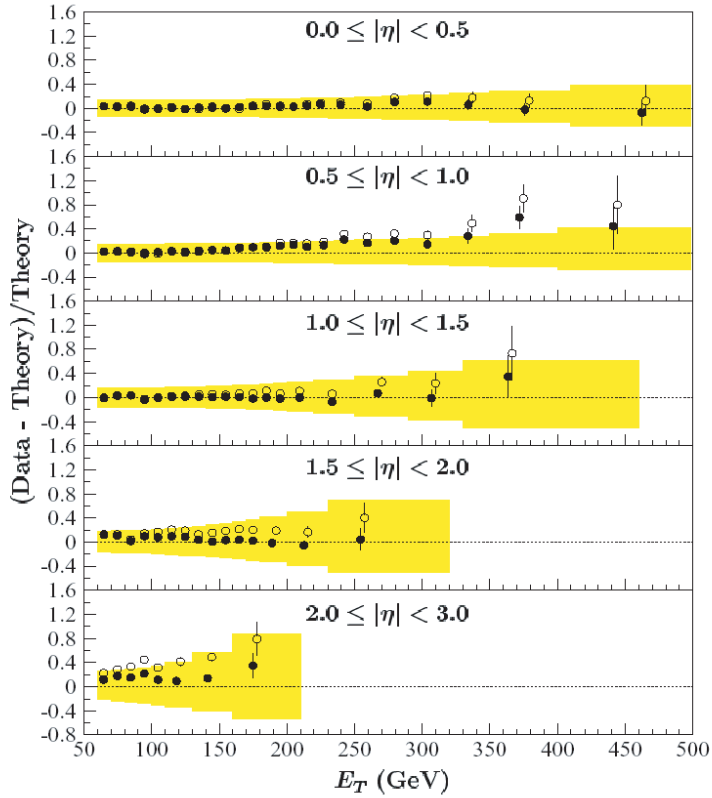


Figure 20: Comparison of $D\bar{O}$ jet data at 1800 GeV from the previous figure with two theoretical models, (\bullet) compares the data to the MRST \uparrow g PDF's while (\circ) compares to the more standard MRST set. The yellow bands indicate the systematic errors, which are completely dominated by the energy scale error.

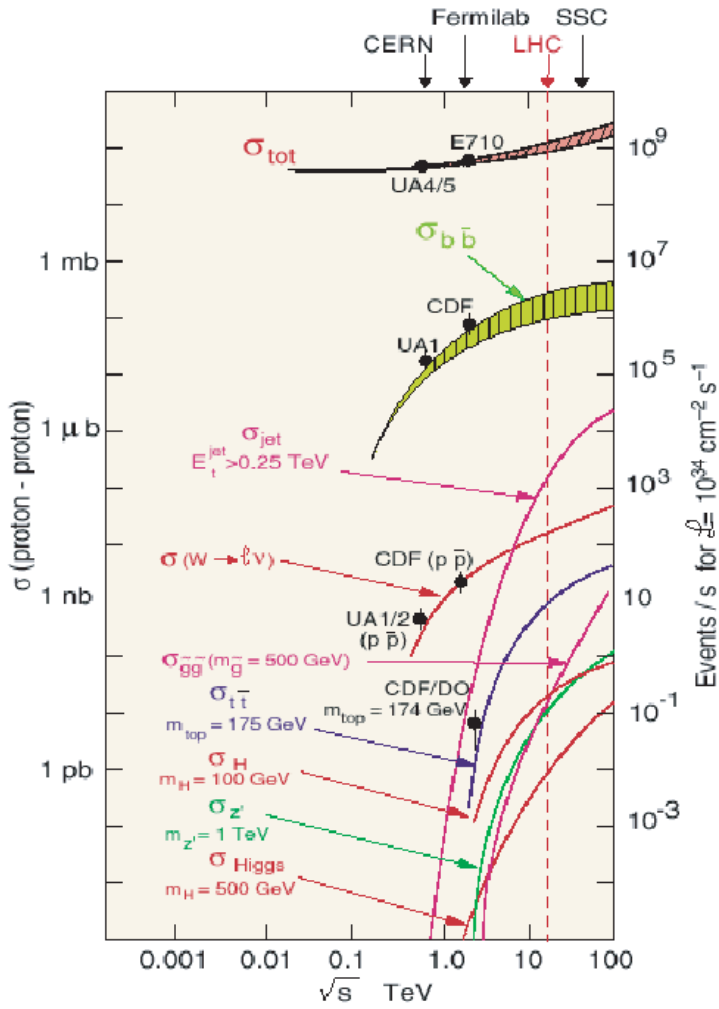


Figure 21: Rates for various processes at Hadron colliders from reference [1]. The dashed vertical line shows the LHC energy. Note the curve labeled $E_T^{jet} > 0.25$ TeV.

- Charm and B decay - a small fraction of jets contain a b or c quark which carries most of the jet energy, the heavy quark can decay semileptonically, producing a muon or electron which carries a large fraction of the jet energy.
- Charge exchange reactions. A charged pion can turn into a neutral pion through a quasi-elastic charge exchange interaction in the calorimeter. This will look identical to an electron, with a charged particle pointing at an electromagnetic shower.

None of these are common - but when one has QCD rates that are thousands of times higher than the signal you are interested in, they become important.

7.2 Discussion of simulations

One way of studying and understanding the backgrounds is to simulate your process, the likely QCD backgrounds and the detector. I'm not going to talk about detector simulations and will concentrate on the methods used as inputs to the detector.

These simulations take the process you are interested in and produce real particles. These simulations differ in two ways from an analytical calculation of a cross section.

First, if you are going to do a detector simulation later on, your physics generator needs to generate real events with real 4-vectors, not just amplitudes or rates. And you get much faster convergence if all events have positive weights and preferably the same weight. Just generating events flat in phase space and then using your analytical calculation to assign a weight to each event is not going to work very well.

Second, nobody knows how to do a perturbative QCD calculation that produces real particles like pions - it would have to be very high order and still could not handle the non-perturbative hadronization phase.

Instead we rely on very useful codes such as PYTHIA [26] and HERWIG [28] which use parton showering or string models to convert partons into particles. These programs manage to simulate many of the interference effects you expect when you have colored particles radiating by using concepts such as angular ordering. Over the past 20 years, the parameters of the models have been tuned to match data from e^-e^+ , lepton-hadron and hadron-hadron scattering.

8 Neutrino detection at colliders

So far we've discussed the detection of electrons, photons and jets. Most interesting high p_\perp processes at colliders involve neutrinos or other non-interacting particles (such as hypothetical Lightest Supersymmetric Particle or LSP). But even high energy neutrinos have a probability of only 10^{-10} of interacting in the typical hadron collider detector. While they cannot be detected, some of their parameters can be estimated by calculating the missing p_\perp in the event.

As noted earlier, we do not know the longitudinal momentum of the scattering quarks but we do have a pretty good idea what their transverse momenta are, close to zero. In principle, if you can measure the transverse momentum of every scattered particle $\vec{p}_\perp^{(i)}$, the transverse momentum of any non-interacting particle will be:

$$\vec{p}_\perp = - \sum_i \vec{p}_\perp^{(i)} \quad (21)$$

The magnitude of this variable is very frequently, and incorrectly, referred to as the missing Transverse Energy, \cancel{E}_\perp or MET. Which is reasonable in the case of a neutrino but just plain wrong in the case of a 70 GeV LSSP or two neutrinos.

The missing transverse momentum estimate only works if the p_\perp and direction of all scattered particles except the missing particle are detected. This requires a 'Hermetic' detector which covers almost all of 4π solid angle with active components. Such coverage is very difficult and expensive to achieve. Detectors such as DØ and CDF have active calorimetry down to angles of order 3° from the beam axis or rapidities out to ± 4 and are able to achieve \cancel{p}_\perp resolutions of order 5 GeV/ c . However there is a potential for very large fluctuations in the missing momentum, for example if a jet fluctuates to be very electromagnetic in a calorimeter which responds differently to hadrons and electrons, exactly the kind of events which fake real electrons.

For events with one missing neutrino from a semi-leptonic decay, such as W boson production, the neutrino reconstruction is almost unambiguous. This is illustrated in Figure 22. However, di-boson production, leptonic top decays and almost any supersymmetric signal have multiple neutral particles in the final state and the missing momentum method can only yield the sum of the missing particles transverse momenta.

9 Example 2: The top quark at the Tevatron

9.1 Standard Model top production

Pairs of top quarks are produced either by quark-antiquark annihilation or gluon-gluon fusion. At the Tevatron, the cross section for this process is believed to be around 7 pb[31]. Single top can also be produced by electroweak diagrams with the exchange of a W but this process has not yet been observed.

As of last year, the DØ and CDF collaborations had recorded an integrated luminosity of over 400 pb $^{-1}$ each in run 1 and 2 combined. This means that the number of top-antitop pairs produced per experiment is:

$$N_{t\bar{t}} = \int \mathcal{L} dt \sigma_{t\bar{t}} = 7\text{pb} * 400\text{pb}^{-1} = 2800 \quad (22)$$

However, at the same time, the total QCD cross section for inelastic scatters is 60 mb.

$$N_{inel} = \int \mathcal{L} dt \sigma_{inel} = 60\text{mb} * 400\text{pb}^{-1} = 2.4 \times 10^{13} \quad (23)$$

So only one in 10^{10} interactions is a top event.

If there are not additional quark species and the CKM matrix is unitary, top is believed to decay .997 of the time to $b + W$ with the W then decaying to $e, \mu, \tau + \nu$ or to $u, c + \bar{d}, \bar{s}, \bar{b}$. Figure 23 illustrates this process. Both kinds of W decay mode are problematic. In the case of leptonic decays, the neutrino leaves the detector without being detected while the hadronic

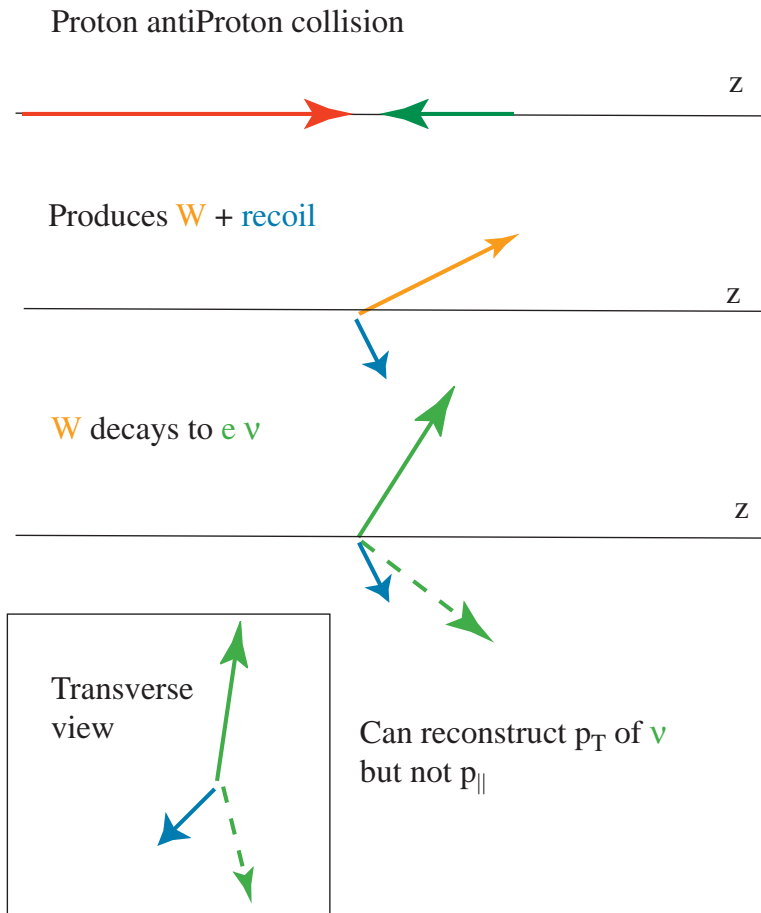


Figure 22: Illustration of W production and decay. The first 3 frames show the longitudinal view. The initial state consists of two quarks with different momenta, so the hard scatter is moving relative to the lab frame. The W is produced with a small recoil and then decays to a neutrino and an electron. The inset frame shows the view along the beam axis. The neutrino's \vec{p}_{\perp} balances the transverse momenta of the recoil and the electron, but there is no information about the longitudinal component of the neutrino momentum.

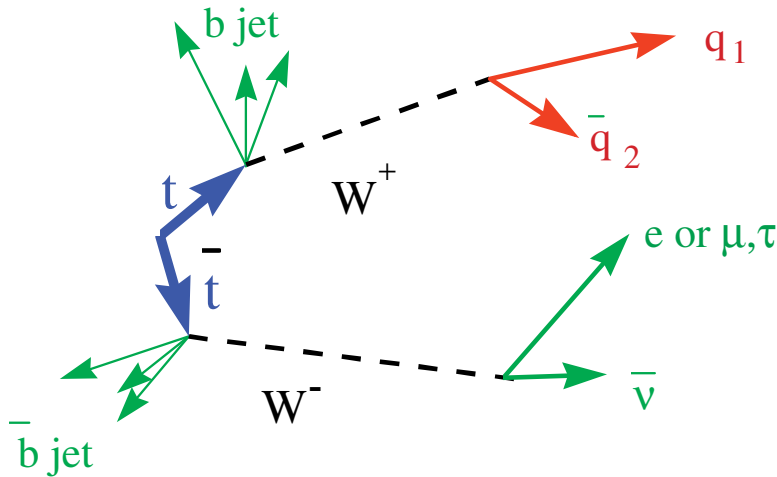


Figure 23: top anti-top production followed by the decays $t \rightarrow bW^+$, $\bar{t} \rightarrow \bar{b}W^-$ with one W decaying leptonically and the other hadronically.

modes look just like the 10^{10} QCD background events. Figure 24 shows the different W^+W^- decay signatures predicted for Standard Model top decays.

9.2 Backgrounds

Typical energies for the leptons and jets produced in top decay are $\frac{m_t}{3}$ or 40-100 GeV and the total energy flowing transverse to the beam direction can be expected to be greater than 200 GeV. The major backgrounds to top production depend on the final state. For the all hadronic final state, the background is QCD going to 6 jets. For the semi-leptonic final states, the QCD/EW process W +jets mimics a top event, or one of the jets from a true QCD event can mimic an lepton and hence a W . The decays with two leptons have much lower backgrounds but are very rare and harder to reconstruct because they have two neutrinos in the final state. For now I am going to concentrate on the semi-leptonic decays which have the signature $t \rightarrow b + \ell\nu$ and $\bar{t} \rightarrow \bar{b} + \bar{q}_1q_2$ (and vice versa). The experimental signature is 4 jets, two of which contain bs while the other two should reconstruct to close to the W mass. The other W decays to a lepton ℓ and missing transverse energy from the neutrino.

One of the major technologies that has made top detection much easier is tagging of b-jets. QCD backgrounds mainly consist of jets initiated by light quarks while top events should have 2 jets containing b quarks. Multi-layer silicon vertex detector with resolutions in the 10-20 μm range allow measurement of the decay length of long lived particles in jets, the presence of a long lived particle is a very strong signature for a b jet and hence a top quark. Figure 25 shows the region within 5 mm of a likely top interaction from CDF which shows two b tags. Figure 26 shows the transverse (xy) decay length distance $L2$ for a set of events from the CDF experiment which have passed all other top cuts. All of the backgrounds have lower $L2$ values than expected for top events.

So we have several experimental handles, the large transverse energy, the presence of a high

W^+W^- decay signatures

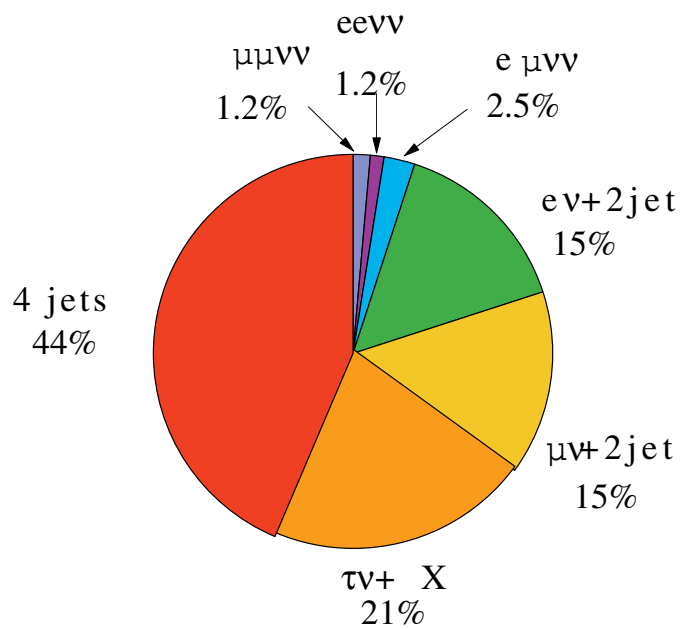


Figure 24: Fraction of $t\bar{t}$ events with different W^+W^- decay signatures. τ decays are lumped together. Note that decay modes involving e or μ^- are a small fraction of the total.

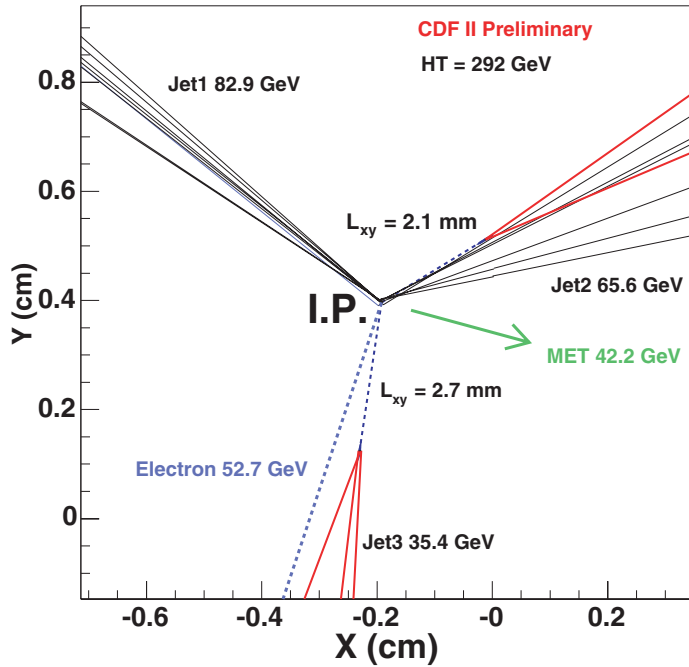


Figure 25: A top -antitop candidate from CDF viewed along the beam axis. Two separated vertices are found which indicate the presence of b-jets from top decay.

p_{\perp} lepton, missing transverse momentum from the neutrino and the b-jets. A combination of all of these can now get a very clean top signal.

Figure 27 shows the number of jets found in CDF events with an identified leptonic W decay from and at least one tagged b jet. For total jet numbers of 3 and 4, the top signal becomes significant.

The CDF collaboration have recently submitted their new measurement of the top cross section in the dilepton channel at 1960 GeV to PRL [32]. It is

$$\sigma_{t\bar{t}} = 7.0 \pm 2.4(stat.) \pm 1.6(syst.) \pm 0.4(lum.) \quad (24)$$

9.3 Top mass

The top mass is one of the most important parameters in the Standard model, because the top quark is heavy enough to have a significant influence on electroweak observables through virtual diagrams. These virtual diagrams lead to correlations between the masses of the W and t and the mass of the Higgs particle. New measurements of the top quark mass from D0's first run were recently published in Nature[34] and CDF have reported but not published results from their most recent running. The interesting part is that improved analysis techniques, better background rejection and calibration improvements have moved the central value to from 174 to 178 ± 4.5 GeV[33]. The effect of this changes is illustrated in Figure 28. The solid green line shows the combined W and top mass measurements from the Tevatron after addition of the more precise D0 measurement. The dashed line shows the previous values.

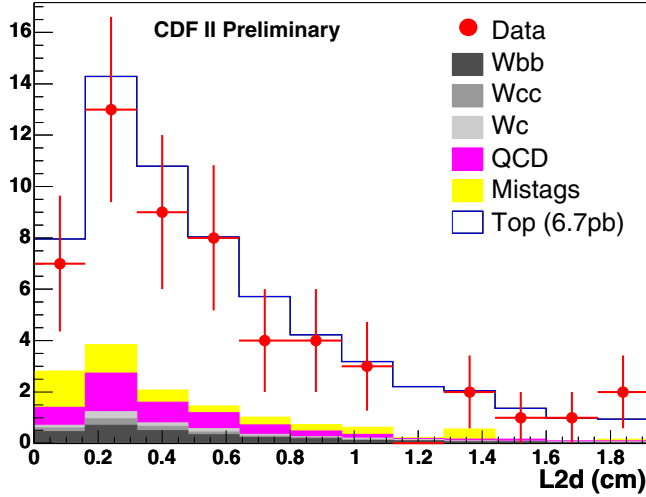


Figure 26: Distribution of the transverse decay length for vertices in b jet candidates from CDF compared to backgrounds.

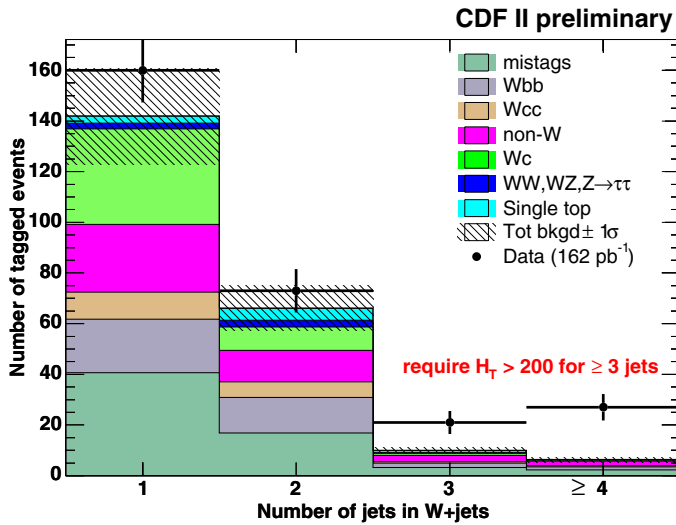


Figure 27: Distribution of the number of jets in addition to a W boson in events with at least one b quark identified by the CDF silicon vertex detector. Top events are expected to have 4 or more jets. A transverse energy cut of 200 GeV has been applied.

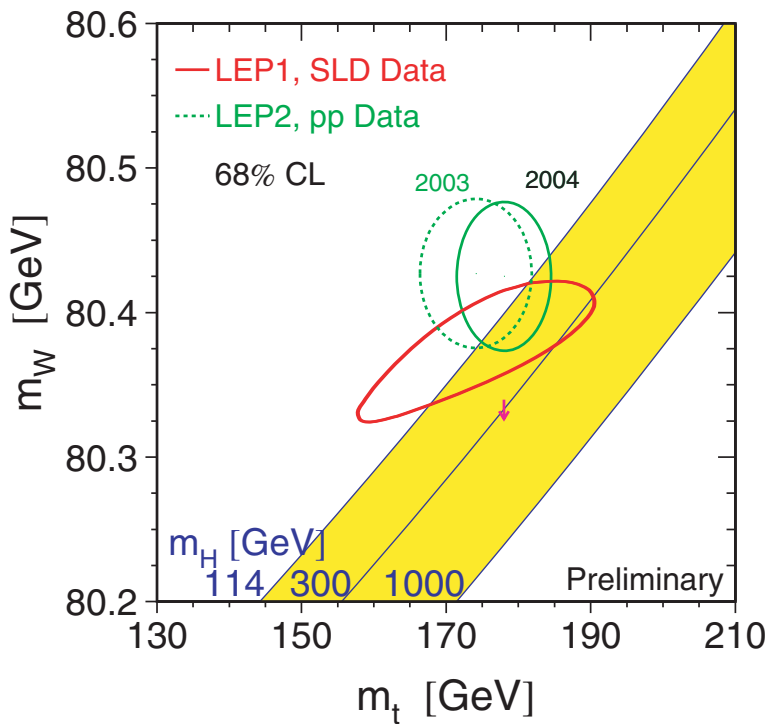


Figure 28: LEPEWWG [24] plot of measurements of electroweak parameters vs. the masses of the top quark and W boson. The yellow bands represent different Standard Model Higgs masses. The solid green line shows the combined W and top mass measurements from the TeVatron after addition of the more precise $D\bar{O}$ measurement. The dashed line shows the previous value.

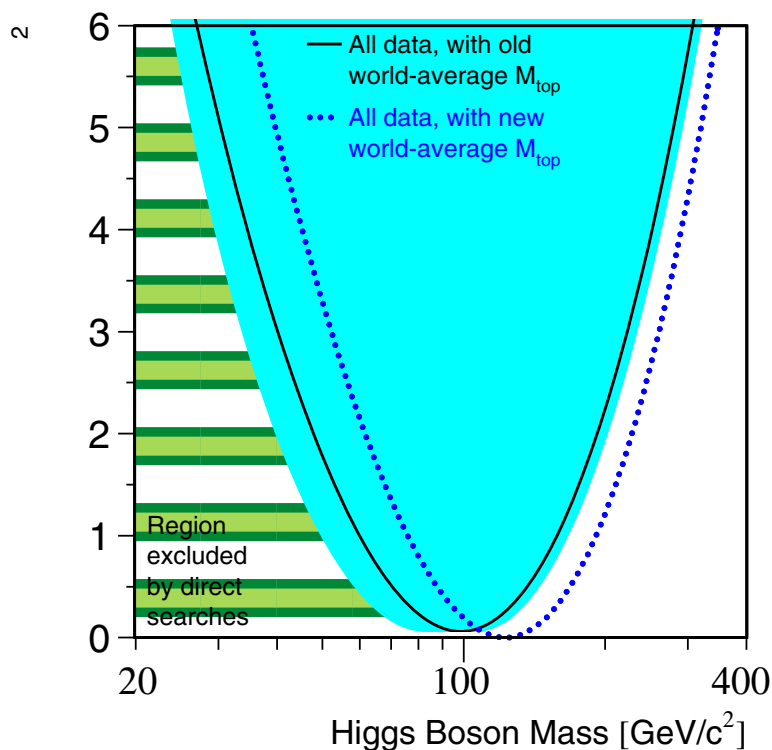


Figure 29: Predictions [24] for the Standard Model Higgs mass. The dark blue dashed parabola shows the new best results with the improved top mass while the black parabola shows the results previous to 2004. The best estimate for the Higgs mass has risen substantially from 96 to 117 GeV/c^2

Figure 29 shows the effect of the change in the central value for the top mass on estimates of the Higgs mass.

9.4 Extraction of the top mass

The top mass can be measured with surprising precision - mainly because it is so high compared to the QCD scale of 1 GeV that strong interaction effects do not dominate, as they do in the determination of the other quark masses.

The basic method goes as follows. We have a top event with one semi-leptonic and 1 hadronic decay.

We know 5 momenta (those of the lepton, 2 jets from W decay and 2 jets from b -decay) and the transverse portion of the neutrino momentum. We also assume that the lepton and neutrino are massless and can estimate the 'masses' of the jets. We can now start applying constraints.

First, the non- b jets come from a W and should have the appropriate mass.

Second, the lepton and neutrino should also reconstruct to the W mass. Here X_{\parallel} is the unknown longitudinal component of the neutrino momentum.

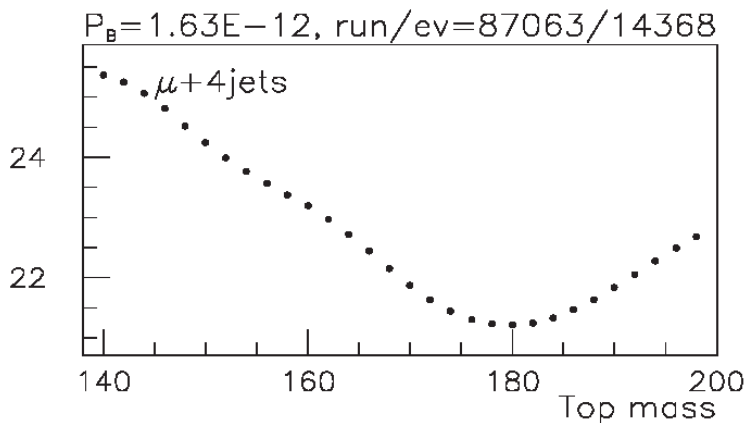


Figure 30: Negative Log Likelihood of the event kinematics for a single event with a very high likelihood of being a top.

$$E_\nu = \sqrt{p_{\perp\nu}^2 + X_{\parallel}^2} \quad (25)$$

$$m_W^2 = (E_\ell + E_\nu)^2 - (\vec{p}_{\perp lepton} + \vec{p}_{\perp\nu})^2 - (p_{\parallel\ell} + X_{\parallel})^2 \quad (26)$$

This is a quadratic equation with two solutions for the neutrino momentum, and hence the W momentum.

We can then impose the remaining constraint, that the masses of the two tops must be equal and extract a top mass.

If detectors were perfect, that would be it but generally, top events have only 1 or zero tagged b jets and the charge of the b jet is not known so it cannot be automatically associated with the W^+ or W^- . In general 12-14 combinations of objects must be considered and their consistency with the top anti-top hypothesis evaluated. In addition, b decays are weak decays and very likely to include neutrinos, which makes the energy determination for b jets different than that for ordinary jets.

Unfortunately, there are also a lot of background events out there as well which cannot be arbitrarily thrown out of the event sample.

The $D\bar{O}$ collaboration very recently published[34] a determination of the top mass using likelihood methods. These methods have an advantage over the techniques used in previous analyses as configurations and events with smaller errors are given greater weight. The data sample used is from the previous run, where vertex tagging was not available to clean up the data sample or indicate which jets contained b quarks. Each combination of particles in each event had its log likelihood of being top or background calculated by comparison to a theoretical model as a function of the top mass. Figure 30 shows this distribution for a single event with a high likelihood for being top. This plot is the sum over all of the combinations. is almost certainly background.

Figure 32 shows the log likelihood distribution for the ensemble of 71 events and the variation of likelihood as a function of the assumed mass near the peak. The optimal value after correction is $m_t = 180.1 \pm 5.3 \text{ GeV}/c^2$. This value is expected to improve greatly once the run II data are well understood as both $D\bar{O}$ and CDF have larger statistics and much better b tagging.

Figure 31: Negative Log Likelihood of the event kinematics for a single event with a very small likelihood of being a top.

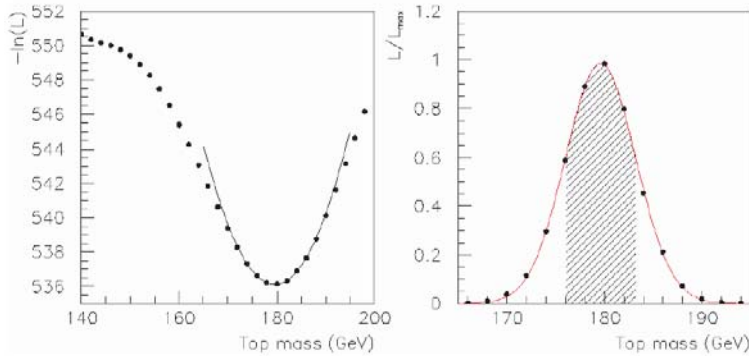


Figure 32: Left: Combined log likelihood function for the 71 events in the sample. Right: the relative likelihoods for the various top masses considered.

The dominant error remains the hadronic energy scale, which should also improve with better top signals as the W bosons in hadronic top decays are indeed the pure calibration line for hadronic energy scales we've needed for a decade.

10 Example 3: looking for the Higgs at Hadron colliders - or where is it anyways?

10.1 Standard Model Higgs production and decay

The Higgs is an excellent example of the difference between production and detection of rare signals. Because the Higgs couples to mass, Standard Model Higgs production generally involves t, W, Z either through loops or direct production. At the Tevatron, low mass Higgs bosons are produced via $GG \rightarrow top\ loop \rightarrow H$ (Figure 33) and associated production (Figure

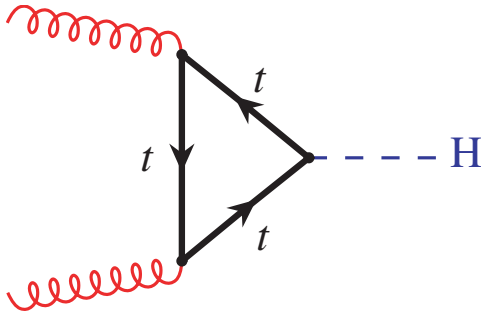


Figure 33: Higgs production by gluon fusion.

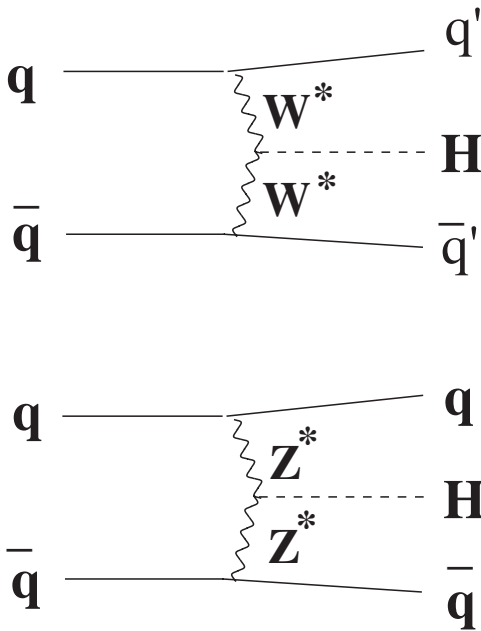


Figure 34: Associated Higgs production.

34 in which a quark and anti-quark produce a W^* which decays to WH . Figure 35 illustrates the relative production rates for these processes [36, 35] at the Tevatron.

The Higgs also likes to decay into the highest mass particles possible. Figure 36 shows the decay modes for low mass Higgs, below WW threshold, the Higgs has to decay to $b\bar{b}$ quarks. So for a Higgs just above the current limit of 114 GeV set by LEP, one would expect a Standard Model cross section for the process $q\bar{q} \rightarrow H \rightarrow b\bar{b}$ of 1 picobarn. During its best week in 2004, the Tevatron recorded over 20 inverse picobarns of data - or enough to produce 20 115 GeV Higgs going into $b\bar{b}$. Even if the Higgs mass were 200 GeV, the cross section for $GG \rightarrow \text{toploop} \rightarrow H \rightarrow WW$ is still over 0.1 picobarn so one would expect to see 2 or 3 in a good week. So why haven't you heard of the discovery or a new limit?

The reason is backgrounds, both due to particle misidentification and real physics processes which have the same final state. In this case, it's likely that real physics is the problem. The total cross section for producing b or \bar{b} quarks at the Tevatron was recently measured by the CDF collaboration [39] in the central (rapidity < 1) region. it is around 25 micro barns, or

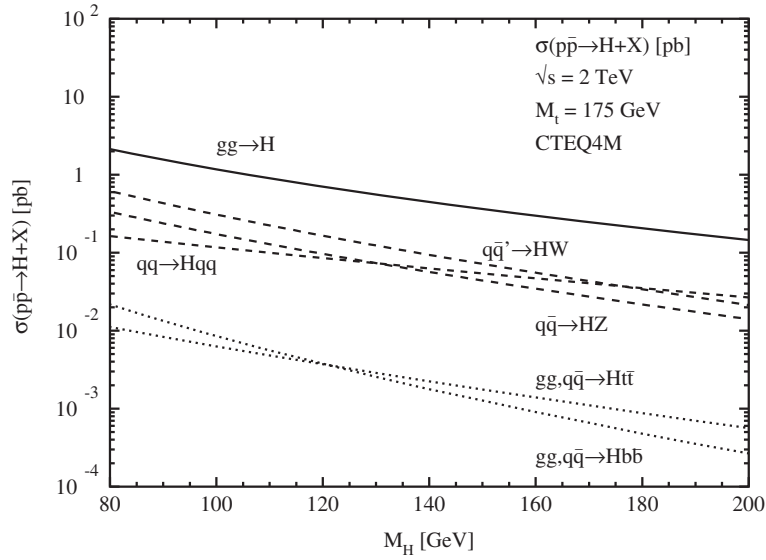


Figure 35: Standard model Higgs cross sections at the Tevatron.

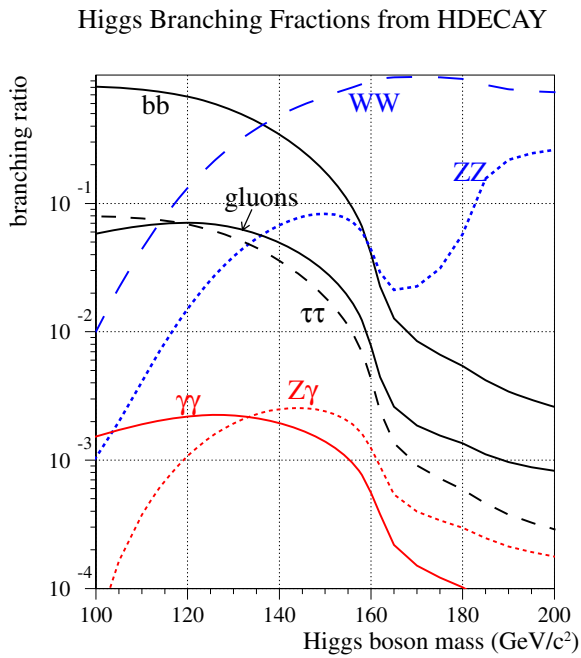


Figure 36: Standard model Higgs decay branching fractions from HDECAY.

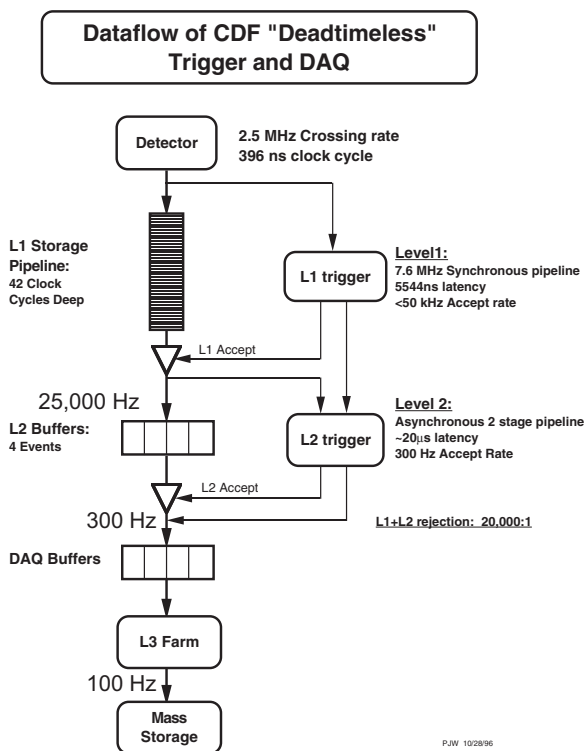


Figure 37: Diagram of the CDF trigger - three levels reduce the data rate from a potential 2.5 MHz to 100 Hz.

around $1/3,000$ of the total proton anti-proton cross section. The cross section for producing $b\bar{b}$ is $1/2$ that, but both CDF and $D\emptyset$ use twice the rapidity range for Higgs analysis as they did for this measurement, so the two factors cancel. This means, at typical luminosities, that 300-500 $b\bar{b}$ pairs are being produced per second, or 10,000,000 times the rate of $H \rightarrow b\bar{b}$. Most such b pairs are highly correlated and have a low invariant mass, but even 1 in a million is enough to swamp the Higgs signal.

10.2 Triggers and Detection

There are also instrumental problems in detecting the $b\bar{b}$ channel. Over 1 million proton-anti-proton interactions occur per second at the Tevatron, but only around 100 can be recorded due to limits on CPU and bandwidth. (Even so the Tevatron fills tapes faster than Fox News does). The rest of the events are eliminated by a multi-level trigger, which tries to distinguish interesting physics (in this case 2 b quarks) from backgrounds (light quark QCD).

CDF has a B physics trigger which relies on detection of the B decay length in the silicon tracker. The $D\emptyset$ B triggers rely more on the detection of muons in semi-leptonic B decay. Figure 37 illustrates the flow of data in the CDF trigger[40]. The Level 1 trigger makes a decision about the usefulness of an event (high energy, has a muon) in 5.5 microseconds. That crude decision takes the raw rate of around 1.5 Million events/second down to around 25,000/second². A Level 2 trigger, which does fast tracking in the silicon detector and detects

²The 45 kHz is a peak number.

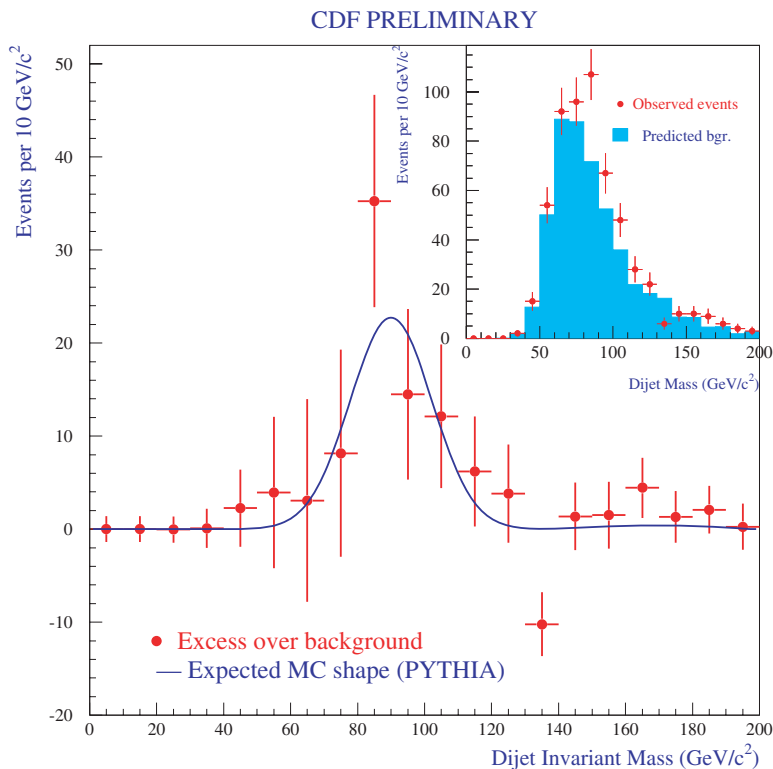


Figure 38: CDF data on the decay $Z \rightarrow b\bar{b}$. The main drawing shows the background subtracted signal and the inset shows the raw data before background subtraction. The points are the data and the histogram is an estimate of the background shape from simulation.

the separated vertex, reduces the data by a further factor of 100 to around 300/second which are then reduced to 100/second by running a full reconstruction program in Level 3. At each stage, real b 's are lost and fake ones can slip through. One can estimate the probability of a simple $b\bar{b}$ event with a large invariant mass surviving by considering the process $q\bar{q} \rightarrow Z \rightarrow b\bar{b}$ which has a cross section of around 15 nanobarns, about half way between the raw $b\bar{b}$ cross section and the Higgs.

Figure 38 shows a previous analysis of $Z \rightarrow b\bar{b}$ from the CDF experiment [39]. This was done with an earlier, less powerful, version of the new trigger and vertex detectors. The Z^0 is the slight enhancement above background on the falling edge of the background. The signal was $91 \pm 30 \pm 19$ events over a background of 250 observed in 110 inverse picobarns of data. This implies that the cross section for *observing* $Z \rightarrow b\bar{b}$ was around 1 picobarn, where the cross section for producing $Z \rightarrow b\bar{b}$ is around 1.5 nanobarns. CDF were only able to detect and identify 1/1,500 of the events with very large backgrounds. One should contrast this with the process $Z \rightarrow ee$ which has 1/5 the production cross section. 3,000 events with less than 1% background were observed in a data sample of similar size. For $Z \rightarrow ee$ the detection probability is of order 10% after triggering and holes in the detector are taken into account. Since those data were taken, CDF has added the separated vertex trigger, which should raise the $Z \rightarrow b\bar{b}$ signal substantially. But even with a good trigger, they won't see the 1 Higgs/week from $GG \rightarrow b\bar{b}$ the Standard Model suggests in our detectors.

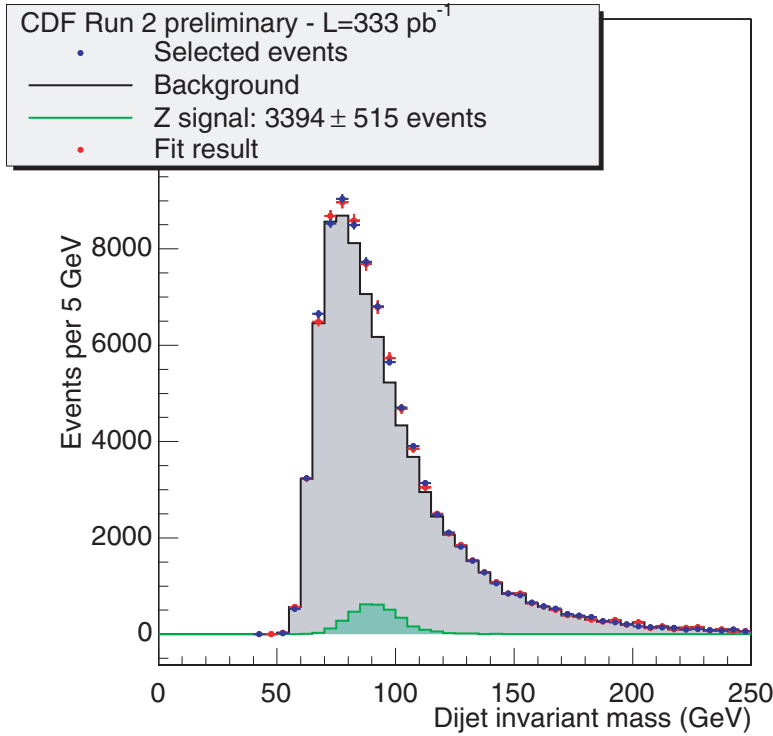


Figure 39: The dijet mass for jets which both contain b mesons from the CDF experiment. The histogram is the estimated background, the small curve at the bottom is the $Z^0 \rightarrow \bar{b}$ signal that results from the fit to the data (which are in blue). The fit to background + $Z^0 \rightarrow \bar{b}$ is in red.

This analysis has been updated with more statistics from Run II and was presented at Moriond QCD this year. Figure Figure 39 shows the new result. The size of the data sample is a factor of 3 larger than in the earlier measurement but in order to increase the signal even further, the efficiency has been increased at the expense of greater backgrounds.

10.3 The solution

There is a solution, look for rarer final states such as $Wb\bar{b}$ from associated production which have much lower backgrounds and higher trigger efficiencies. In particular, the presence of the W eliminates the need to trigger on a b quark. Figure 40 shows the data and background/signal sources for $Wb\bar{b}$ production at the DØ detector which was recently submitted to PRL [42]. The dominant backgrounds are real $W+$ continuum $b\bar{b}$ and top production. The limit set on Higgs production is around 10 times the expected Standard Model cross section. The Tevatron Higgs Sensitivity study [35] done in 2003, indicated that integrated luminosities of 5,000-10,000 inverse picobarns will be necessary to see a Standard Model Higgs at the Tevatron.

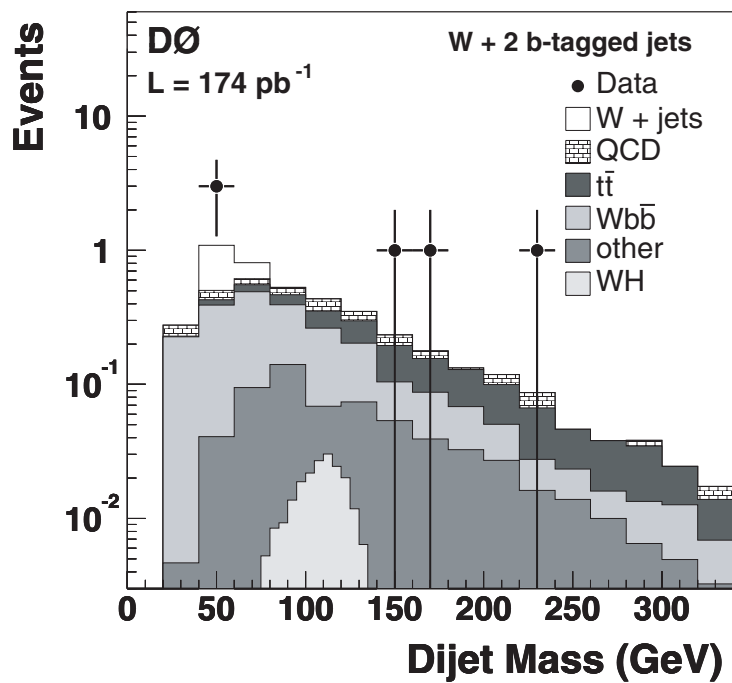


Figure 40: Invariant mass of $H \rightarrow b\bar{b}$ candidates in the D0 detector. The points show the 5 data events while the histograms show various sources of backgrounds. The bump at the bottom is the signal expected from a Standard Model Higgs of mass 115 GeV.

11 Conclusions

I've discussed how particle detectors work at hadron colliders and the signatures for old and new physics. I've emphasized the problems in extracting rare signals from a very large background. I'll end with some advice for the aspiring theorist who wishes to have his/her ideas tested in the next 20 years.

- Rate alone cannot guarantee that a process you predict will be detectable.
- The key is special signatures - final state electrons, muons, taus, heavy quarks, which are harder for QCD processes to mimic.
- To find truly rare processes, you probably need to use multiple special signatures.
- Get experimentalists interested in your physics - so they don't throw it out at Level 1 in their trigger.

References

- [1] C. Bernardini, *Phys. Perspect.* **6**, 156 (2004).
- [2] Section 26. "High-energy colliders", Review of Particle Properties - K. Hagiwara et al., *Phys. Rev. D* **66**, 010001 (2002).
- [3] R. Assmann *et al.*, "Calibration of centre-of-mass energies at LEP1 for precise measurements of Z properties," *Eur. Phys. J. C* **6**, 187 (1999).
- [4] [LEP Collaborations], "Combination procedure for the precise determination of Z boson parameters from results of the LEP experiments," arXiv:hep-ex/0101027.
- [5] R. Akers *et al.* [OPAL Collaboration], "Improved measurements of the neutral current from hadron and lepton production at LEP," *Z. Phys. C* **61**, 19 (1994).
- [6] G. Abbiendi *et al.* [OPAL Collaboration], "Precision luminosity for Z0 lineshape measurements with a silicon-tungsten calorimeter," *Eur. Phys. J. C* **14**, 373 (2000) [arXiv:hep-ex/9910066].
- [7] M. Browne, "315 Physicists Report Failure in Search for Supersymmetry," *New York Times*, January 5, 1993.
- [8] T. Sjöstrand, P. Edén, C. Friberg, L. Lönnblad, G. Miu, S. Mrenna and E. Norrbin, *Computer Physics Commun.* **135** (2001) 238. and hep-ph/0108264.
- [9] <http://www.phys.psu.edu/~cteq/handbook/v1.1/handbook.pdf>
- [10] R. Schwitters, "Jet Production in High Energy Hadron Collisions", Proceedings of the 11th Slac Summer Institute, P. McDonough editor, SLAC Report 267, 1984.
- [11] Review of Particle Properties - K. Hagiwara et al., *Phys. Rev. D* **66**, 010001 (2002)
- [12] R. M. Snihur, "Subjet Multiplicity Of Quark And Gluon Jets Reconstructed With The K(T) Algorithm In P Anti-P Collisions," Northwestern University Doctoral Dissertation, FERMILAB-THESIS-2000-25,
- [13] D. Denegri, Standard Model physics at the LHC (pp collisions), 27 November 1990, Proceedings of the Large Hadron Collider Workshop, Aachen, 4-9 October 1990, Vol I,II,III, CERN 90-10.

- [14] Jay Dittman, Talk given at the Jet/Met workshop at Fermilab, January 28, 2004. <http://agenda.cern.ch/fullAgenda.php?ida=a04329> .
- [15] B. Abbott *et al.* [D0 Collaboration], “Inclusive jet production in p anti-p collisions,” Phys. Rev. Lett. **86**, 1707 (2001) [arXiv:hep-ex/0011036], V. M. Abazov *et al.* [D0 Collaboration], “Multiple jet production at low transverse energies in p anti-p collisions at $s^{*(1/2)} = 1.8\text{-TeV}$,” Phys. Rev. D **67**, 052001 (2003) [arXiv:hep-ex/0207046]
- [16] J. C. Estrada Vigil, “Maximal Use Of Kinematic Information For The Extraction Of The Mass Of The Top Quark In Single-Lepton T Anti-T Events At D0,” Univ. of Rochester Doctoral Dissertation, FERMILAB-THESIS-2001-07,
- [17] M. F. Canelli, “Helicity of the W boson in single-lepton t anti-t events,” FERMILAB-THESIS-2003-22
- [18] B. Abbott *et al.* [D0 Collaboration], “Determination of the absolute jet energy scale in the D0 calorimeters,” Nucl. Instrum. Meth. A **424**, 352 (1999) [arXiv:hep-ex/9805009].
- [19] L. R. Babukhadia, “Rapidity Dependence Of The Single Inclusive Jet Cross-Section In Proton - Anti-Proton Collisions At The Center-Of-Mass Energy Of 18-Tev With The D0 Detector,” , University of Arizona Doctoral Dissertation, FERMILAB-THESIS-1999-03,
- [20] T. Affolder *et al.* [CDF Collaboration], Phys. Rev. D **64**, 032001 (2001) [Erratum-ibid. D **65**, 039903 (2002)] [arXiv:hep-ph/0102074].
- [21] S. Frixione and B. R. Webber, “Matching NLO QCD computations and parton shower simulations,” JHEP **0206**, 029 (2002) [arXiv:hep-ph/0204244]. S. Frixione and B. R. Webber, “The MC@NLO 2.3 event generator,” arXiv:hep-ph/0402116.
- [22] M. Kramer and D. E. Soper, “Next-to-leading order QCD calculations with parton showers. I: Collinear singularities,” Phys. Rev. D **69**, 054019 (2004) [arXiv:hep-ph/0306222].
- [23] S. Mrenna and P. Richardson, “Matching matrix elements and parton showers with HERWIG and PYTHIA,” JHEP **0405**, 040 (2004) [arXiv:hep-ph/0312274].
- [24] T. Sjostrand, L. Lonnblad, S. Mrenna and P. Skands, “PYTHIA 6.3: Physics and manual,” arXiv:hep-ph/0308153. T. Sjostrand, P. Eden, C. Friberg, L. Lonnblad, G. Miu, S. Mrenna and E. Norrbin, “High-energy-physics event generation with PYTHIA 6.1,” Comput. Phys. Commun. **135**, 238 (2001) [arXiv:hep-ph/0010017].
- [25] T. Affolder *et al.* [CDF Collaboration], “Charged particle multiplicity in jets in p anti-p collisions at $s^{*(1/2)} = 1.8\text{-TeV}$,” Phys. Rev. Lett. **87**, 211804 (2001).
- [26] G. Corcella *et al.*, “HERWIG 6: An event generator for hadron emission reactions with interfering JHEP **0101**, 010 (2001) [arXiv:hep-ph/0011363]. G. Marchesini, B.R. Webber, G. Abbiendi, I.G. Knowles, M.H. Seymour and L. Stanco, Computer Phys. Commun. **67** (1992) 465.
- [27] Jason Nielsen, talk at the 2004 Lake Louise Winter Institute;
- [28] <http://www-cdf.fnal.gov/physics/top/RunIIWjets/webpages/secvtx/public.html>
- [29] M. Cacciari, S. Frixione, M. L. Mangano, P. Nason and G. Ridolfi, “The t anti-t cross-section at 1.8-TeV and 1.96-TeV: A study of the systematics due to parton densities and scale dependence,” JHEP **0404**, 068 (2004) [arXiv:hep-ph/0303085].

- [30] D. Acosta *et al.* [CDF Collaboration], “Measurement of the t anti-t production cross section in p anti-p collisions at $s^{**}(1/2) = 1.96\text{-TeV}$ using dilepton events,” arXiv:hep-ex/0404036.
- [31] Lep Electroweak Working group and Tevatron Electroweak working group, <http://lepewwg.web.cern.ch/LEPEWWG/>, <http://tevewwg.fnal.gov/>
- [32] V. M. Abazov *et al.* [D0 Collaboration], “A precision measurement of the mass of the top quark,” *Nature* **429**, 638 (2004).
- [33] L. Babukhadia *et al.* [CDF and D0 Working Group Members Collaboration], “Results of the Tevatron Higgs sensitivity study,” FERMILAB-PUB-03-320-E
- [34] T. Han and S. Willenbrock, “QCD correction to the $p p \rightarrow W H$ and $Z H$ total cross-sections,” *Phys. Lett. B* **273**, 167 (1991).
- [35] A. Djouadi, J. Kalinowski and M. Spira, “HDECAY: A program for Higgs boson decays in the standard model and its supersymmetric extension,” *Comput. Phys. Commun.* **108**, 56 (1998) [arXiv:hep-ph/9704448].
- [36] M. Spira, “Higgs boson production and decay at the Tevatron,” arXiv:hep-ph/9810289.
- [37] P. J. Bussey [CDF Collaboration], “Charm and beauty production at CDF,” arXiv:hep-ex/0408020. M. Cacciari, S. Frixione, M. L. Mangano, P. Nason and G. Ridolfi, “QCD analysis of first b cross section data at 1.96-TeV,” *JHEP* **0407**, 033 (2004) [arXiv:hep-ph/0312132].
- [38] S. Baroiant *et al.* [CDF-II Collaboration], “The CDF-II tau physics program: Triggers, tau ID and preliminary results,” arXiv:hep-ex/0312020.
- [39] T. Dorigo [CDF collaboration], “Observation of Z decays to b quark pairs at the Tevatron collider,” arXiv:hep-ex/9806022.
- [40] V. M. Abazov *et al.* [D0 Collaboration], arXiv:hep-ex/0410062.